Received: 25 May 2021 | Revised: 21 September 2021 | Accepted: 24 September 2021

DOI: 10.1002/esp.5274

RESEARCH ARTICLE

ESPL WILEY

Spatial and temporal controls on proglacial erosion rates: A comparison of four basins on Mount Rainier, 1960 to 2017

Scott W. Anderson[1] | David Shean[2]

[1]US Geological Survey, Washington Water Science Center, Tacoma, Washington, USA

[2]Civil and Environmental Engineering, University of Washington, Seattle, Washington, USA

Correspondence
Scott W. Anderson, US Geological Survey, Washington Water Science Center, Tacoma, WA 98402, USA.
Email: swanderson@usgs.gov

Funding information
King County, WA; U.S. Geological Survey

Summary

The retreat of alpine glaciers since the mid-19th century has triggered rapid landscape adjustments in many headwater basins. However, the degree to which decadal-scale glacier retreat is associated with systematic or substantial changes in overall coarse sediment export, with the potential to impact downstream river dynamics, remains poorly understood. Here, we use repeat topographic surveys to assess geomorphic change in four partly glaciated basins on a stratovolcano (Mount Rainier) in Washington State at roughly decadal intervals from 1960 to 2017. The proglacial extents of the four basins show distinct geomorphic trajectories, ranging from substantial and sustained net erosion to relatively inactive with net deposition. These different trajectories correspond to differences in initial (1960) valley floor gradients, and can be effectively understood as valley floor grade adjustments. Significant erosion was most often accomplished by debris flows triggered by extreme rainfall or glacial outburst floods, though a single rockfall mobilized more material than all other events combined. Year-to-year runoff events had little measurable geomorphic impact. Exported material tended to accumulate in broad deposits within several kilometers of source areas and largely remained there through the end of the study period. Over 10- to 100-year timescales, we find that the impact of glacier retreat on coarse sediment yield may then vary substantially according to the geometry and storage trends of the newly exposed valley floor; the timing of that response may also be dictated, and potentially obscured, by stochastic and/or extreme events.

KEYWORDS

topographic change, sediment transport, proglacial, paraglacial, photogrammetry, Mount Rainier

1 | INTRODUCTION

Glaciers around the world have generally been retreating since the mid-19th century (Leclercq et al., 2014), and most are expected to continue retreating for the foreseeable future (Hock et al., 2019). This retreat has triggered geologically rapid landscape adjustments in many headwater basins, as glacially formed landscapes have been progressively reshaped by subaerial processes of mass wasting and fluvial sediment transport (Cossart & Fort, 2008; Curry et al., 2006; Heckmann et al., 2016; Lane et al., 2017; Shugar et al., 2017). However, the overall change in headwater clastic sediment export associated with these landform adjustments often remains unknown; this is particularly true in terms of the export of coarse sediment (coarse sand to boulders) that typically makes up the mobile channel bed of downstream river systems (though see Comiti et al., 2019; Lane et al., 2017; Micheletti & Lane, 2016). To date, it then remains difficult to predict whether recent or future glacier retreat, by affecting changes in coarse sediment export from glaciated watersheds, is likely to have a substantial or predictable impact on river planform, elevation, or bed material fluxes in reaches well beyond the immediate proglacial forefield.

Discussions of geomorphic responses to recent deglaciation (e.g., Cossart & Fort, 2008; Knight & Harrison, 2018; Lane et al., 2017; Orwin & Smart, 2004) have often been grounded in the concept of a paraglacial landscape response in which the exposure of mobile glacial sediments results in a transient period of increased sediment yield

(Ballantyne, 2002a, 2002b; Church & Ryder, 1972; Ryder 1971). The notion of a paraglacial period has provided a robust explanation for observed sediment yields over glacial–interglacial timescales (e.g., Brardinoni et al., 2018) and/or large (regional to continental) spatial scales (e.g., Church & Slaymaker, 1989), as well as for the evolution of individual landforms (e.g., Curry et al., 2006). However, studies of decadal-scale proglacial or paraglacial sediment dynamics have tended to highlight the substantial local and short-term complexity of sediment transfers through these landscapes. Consistent themes in those studies include the key role of storage and connectivity as controls on if, how, or when exposed sediment is ultimately exported (Cavalli et al., 2019; Cossart, 2008; Cossart & Fort, 2008; Heckmann & Vericat, 2018; Meigs et al., 2006; Micheletti et al., 2015; Turley, 2020) and the importance of infrequent extreme events on overall sediment export (Carrivick & Rushmer, 2009; Micheletti & Lane, 2016; Xu et al., 2015). Taken together, results to date suggest that, over periods of decades to centuries, the relation between glacier retreat and watershed-scale coarse sediment yield may be complex in both space and time (Cossart, 2008; Cossart et al., 2018), similar to findings for the finer fraction of exported sediment (Leonard, 1997; Menounos & Clague, 2008).

In recent decades, the use of repeat high-resolution topographic surveys has provided an increasingly practical tool for observing subaerial sediment transfers, and such surveys have become a mainstay of proglacial sediment studies (Anderson & Jaeger, 2020; Anderson & Pitlick, 2014; Betz et al., 2019; Carrivick et al., 2013; Comiti et al., 2019; Delaney et al., 2018; Heckmann & Vericat, 2018; Lane et al., 2017; Schiefer & Gilbert, 2007; Smith et al., 2006). The dramatic increase in accessible photogrammetric methods, coupled with archives of scanned aerial imagery often extending back to the 1950s, has further opened up the potential for analyzing high-resolution change prior to the advent of modern laser scanning methods (Micheletti et al., 2015). The combination of limited vegetation, large scales of geomorphic change, and coarse surface textures make proglacial areas particularly well suited to these photogrammetric approaches to digital elevation model (DEM) derivation and change analysis (Schiefer & Gilbert, 2007).

Here, we use a large collection of topographic datasets, derived from historical aerial imagery, satellite imagery, and aerial lidar collected between 1960 and 2017, to assess geomorphic change in four deglaciating watersheds on a stratovolcano (Mount Rainier) in the Cascade Range of Washington State (Figure 1). The goals of this study are to (1) document rates and processes of proglacial or glacier-marginal erosion over past 60 years; (2) explore controls on those rates over time and across different basins; and (3) to the degree allowed by the data, assess the downstream fate of material mobilized beyond the proglacial limits. This study is largely motivated by an interest in how changing sediment delivery from parts of the landscape exposed through glacier retreat since the 19th century may impact river channel dynamics at points farther downstream. "Reaches downstream" include both the high-gradient reaches immediately below the proglacial zone as well as lower gradient reaches adjacent to population centers in the Puget Lowlands (Figure 1, inset). As such, we focus here on the overall rate at which material is mobilized beyond the proglacial zone, as opposed to detailing the evolution of individual landforms or sediment transfers within the proglacial zone.

2 | STUDY AREA

Mount Rainier is a stratovolcano in Washington State composed of stratified andesite and dacite lavas, with a summit elevation of 4392 m (Driedger & Kennard, 1986; Reid et al., 2001). Mount Rainier is home to Mount Rainier National Park and hosts the headwaters of multiple river systems that drain out to the populated Puget Lowlands (Figure 1). Prior studies of recent proglacial sediment processes on Mount Rainier have tended to focus on the Tahoma Creek watershed, which has produced the majority of recorded debris flows on Mount Rainier over the past half-century (Anderson & Pitlick, 2014; Driedger & Fountain, 1989; Turley, 2020; Walder & Driedger, 1994), or the spatial distribution and initiation of debris flows over the past decade (Copeland, 2009; Legg et al., 2014). (For this paper, we use "debris flow" to refer specifically to hydrologically triggered, non-cohesive debris flow events that have been observed over the historical record in proglacial environments. We use the term "lahar" somewhat informally to refer to much larger debris flow events associated with large-scale collapse of the volcanic edifice; see Scott et al. (1995) for more discussion of these terms). These debris flows are generally assumed to be the primary means by which proglacial and glacier-marginal sediments are transferred farther downvalley. In addition to debris flows, the sediment flux at the study basin outlets is complemented by the fluvially transported load, including large volumes of fine sediment sourced from under and within glaciers. Finally, over longer timescales, episodic rockfalls and lahars may transfer immense volumes of material downvalley, with some lahar deposits extending to Puget Sound (Scott et al., 1995). For detailed discussions of the full sediment cascade at Mount Rainier, with a focus on contemporary processes, see Czuba et al. (2012) and Turley (2020).

This study focuses on four glacier/proglacial systems: the Nisqually Glacier, which feeds into the Nisqually River; the South Tahoma Glacier, which feeds into Tahoma Creek (this basin also includes a tongue of the Tahoma Glacier, which historically merged with the South Tahoma Glacier); the Emmons Glacier, which feeds into the White River; and the Winthrop Glacier, which feeds into the West Fork White River (Figures 1 and 2 and Table 1). The Nisqually and South Tahoma glaciers are both south-facing and part of the larger Nisqually River watershed. The Emmons and Winthrop glaciers are both north-facing and both part of the White River watershed (Figure 1). For each study basin, our primary area of interest was defined as the contributing area of the main stream at the distal limits of the 19th-century glacial maxima. These watersheds are largely composed of the contemporary glacier and the associated proglacial zone, but also include unglaciated areas adjacent to the primary proglacial extents. Following the convention presented in Heckmann et al. (2016), the proglacial zone was defined by the the maximum extent of 19th-century glaciation, as inferred from dated moraines and trimlines in the modern landscape (Sigafoos & Hendricks, 1972).

In general, subaerial geomorphic activity predominately occurred within the proglacial limits as defined by Heckmann et al. (2016), and our study can largely be viewed as a study of proglacial processes. The area around the Winthrop Glacier presents a unique case, in that most geomorphic activity has occurred in a series of channels running immediately outboard of the western 19th-century moraines (Figure 2d). These channels typically drain unglaciated slopes to the west of the glacier, but glacial outburst floods appear to episodically

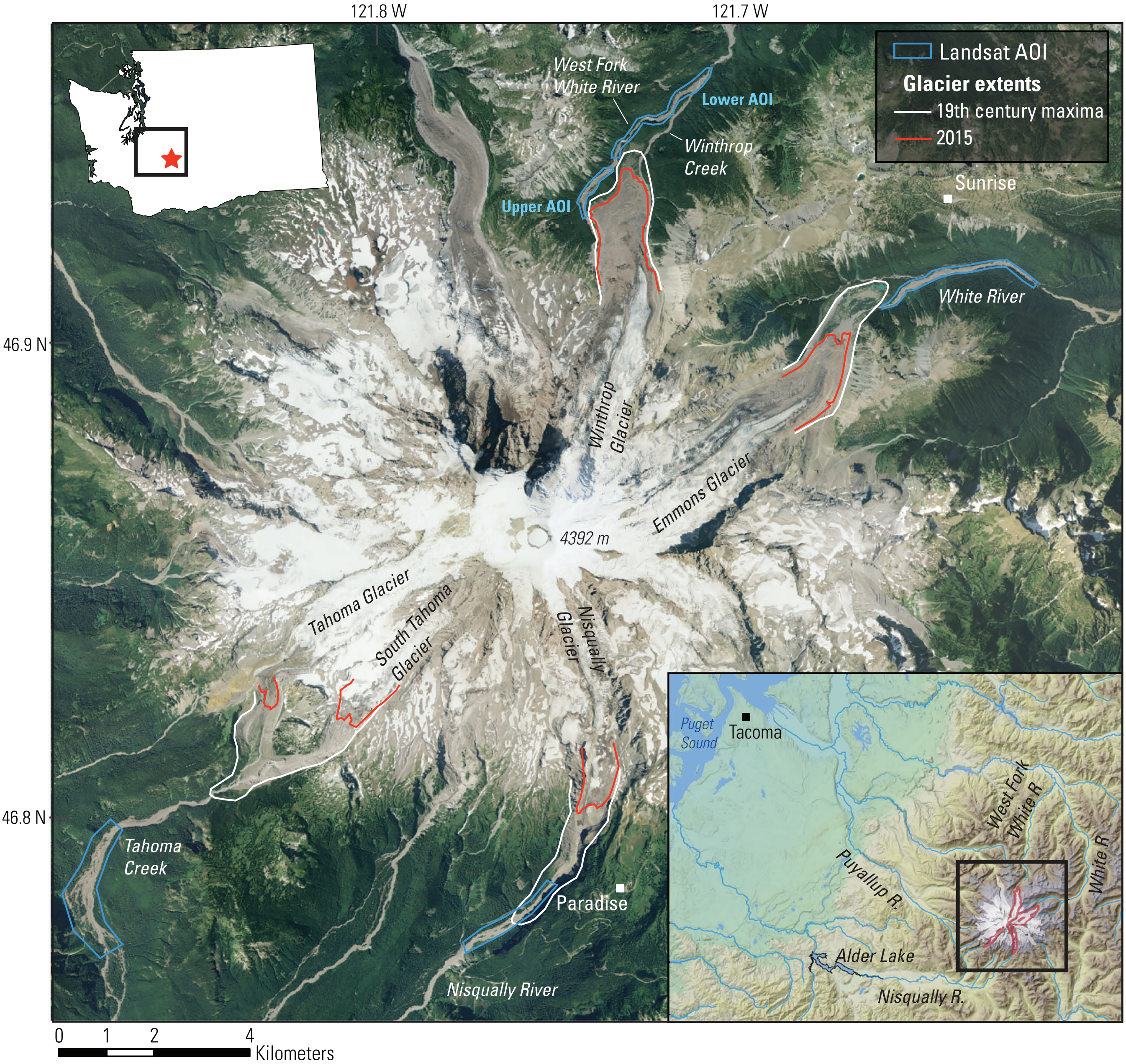

FIGURE 1 Overview of Mount Rainier study area, with glacier extents for study basins. Base imagery in main panel is aerial imagery from 2009 collected through the National Agriculture Imagery Program. Glacier extents at 19th-century maxima are from Sigafoos and Hendricks (1972); glacier extents from 2015 were provided by Beason (2017). Polygons defining areas used in Landsat analysis are indicated in blue

flow down them. These channels contain the West Fork White River proper, while the actual outlet of the Winthrop Glacier (Winthrop Creek) is considered a short tributary of that river (Figure 1). For the Winthrop Glacier basin, we define our study area as the combined contributing areas of both the West Fork White River and Winthrop Creek at the approximate maximum downvalley extent of 19th-century glaciation.

By virtue of sitting on the flanks of a stratovolcano near the coast, the proglacial settings on Mount Rainier have some distinct characteristics when compared to proglacial settings in the European Alps or Arctic regions. First, valley geometries tend to be relatively simple; most basins are radially oriented around the peak, with a single glacier feeding into a trunk valley river system and bordered by unglaciated slopes (Figure 2). Second, the flanks of Mount Rainier, and the glaciers resting on them, are steep and generally become steeper moving upslope, lacking the cirques common in many alpine settings. Although proglacial lakes do occur in the Cascade Range (O'Connor & Costa, 1993), no such lakes of any size currently exist in any of the study watersheds. Third, the proximity to coastal moisture and the substantial orographic lift provided by the peak means the flanks of Mount Rainier are subject to large fall and winter rain storms. These fall and winter storms typically produce the largest floods in a given year, and major rain events regularly produce floods an order of magnitude larger than summer melt peaks.

Lastly, many basins have experienced periodic outburst floods, associated with the rapid release of englacially or subglacially stored water (Driedger & Fountain, 1989). Outburst events tend to occur in the summer or early fall during periods of warm weather or punctuated rainfall (Walder & Driedger, 1995), and there is an anecdotal association between stagnant ice and outburst floods. However, the

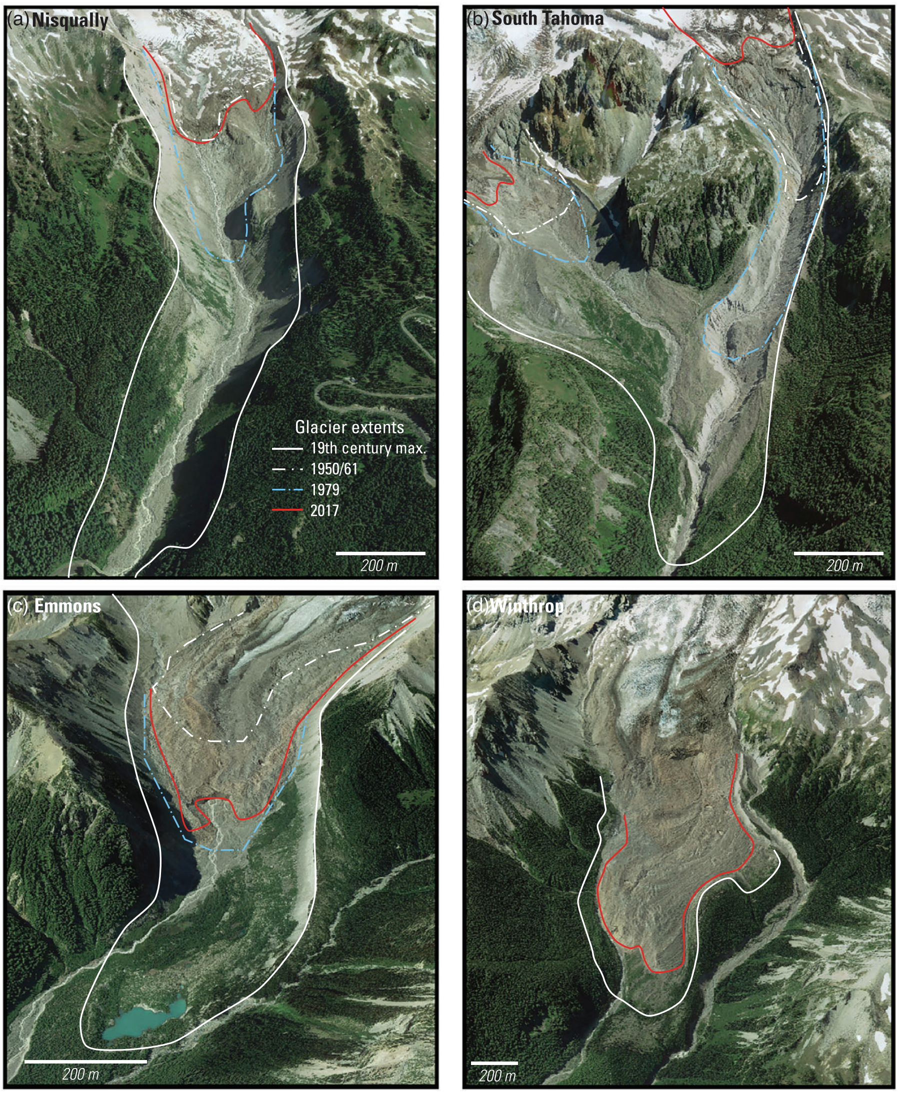

FIGURE 2 Oblique renderings of (a) the Nisqually Glacier and proglacial zone, (b) the South Tahoma Glacier and proglacial zone, (c) the Emmons Glacier and proglacial zone, and (d) the Winthrop Glacier proglacial zone. Base imagery is 25 July 2018, imagery obtained from Google Earth. Glacier extents at 19th-century maxima are from Sigafoos and Hendricks (1972). All other glacier extents were digitized directly from imagery used in this study. The extents of the Winthrop Glacier have not changed markedly since the 1960s, and so only the 19th-century maxima and 2017 outlines are shown here

TABLE 1 Glacier and proglacial metrics for study basins

	Glacier area (km^2)		Deglaciated area (km^2)		Terminus elevation (m)	
Study area	1951/60	2017	1960	2017	1960	2017
South Tahoma[a]	3.7	3.2	0.9	1.4	1660	2090
Nisqually	6.0	5.7	1.8	2.1	1470	1650
Winthrop[b]	8.7	8.7	0.7	0.7	1480	1480
Emmons	11.6	12.2	2.1	1.5	1580	1500

[a]South Tahoma areas do not include glacier or proglacial area associated with the Tahoma Glacier.
[b]Winthrop deglaciated area does not include channel areas to the west of glacier extents.

mechanics of these outburst events remain poorly understood. Outburst events are primarily of interest due to their propensity to trigger debris flows; the actual volumes of water released during outburst floods appear to be relatively modest and are generally not associated with substantial water floods.

2.1 | Changes in glacier extent

In the mid-19th century, glaciers on Mount Rainier were at or near their most advanced state of the past several thousand years, and have generally been retreating since (Sigafoos & Hendricks, 1972). Terminus retreat rates accelerated from the 1920s through the 1940s, followed by a period of readvances starting in the 1950s (Nylen, 2004). Those readvances continued through the 1970s for the south-facing glaciers, and extended into the 1990s for the north-facing glaciers. Similar trends have been observed on other stratovolcanoes in the region and the general timing of major mass-balance shifts match global glacier trends over the past century (Dick, 2013; Zemp et al., 2009).

Most of the glacier area loss since 19th-century maxima occurred prior to 1940 at these sites. Mid-century readvances were substantial enough that, despite steady retreat in recent decades, glacier extents in 2017 are often similar to minima seen in the 1950s (Figure 2). The period of topographic record used here (1960–2017) then starts in the middle of that mid-century readvance, and extends over a period in which retreat has exposed parts of the landscape previously exposed in the first half of the 20th century.

2.2 | The 2006 storm

Over 6–7 November 2006, a large atmospheric river trained directly at Mount Rainier dropped roughly 500 mm of rain over the peak (Konrad & Dettinger, 2017; Legg et al., 2014). Debris flows, landslides, and river channel migration caused widespread damage to National Park infrastructure. The 3-day total precipitation associated with this storm was the largest since records began in 1920, and by a large margin (Figure 3). This storm occurred prior to any significant seasonal snow accumulation, with rain falling directly on bare slopes. Compared against the subset of rain events impacting snow-free slopes, 3-day total precipitation during the 2006 event was almost an order of magnitude larger than typical years (Figure 3d). The intensity of this storm makes it a prominent feature in the analyses that follow.

3 | METHODS

3.1 | DEM generation

Most of the topographic data used in this study were derived using Structure from Motion (SfM) photogrammetric methods applied to historical aerial imagery (Figure 4 and Table 2). The majority of that imagery was collected by the US Geological Survey between 1967 and 1994 as part of the North American Glacier Aerial Photography (NAGAP) program (Post, 1995), and later scanned and archived by Nolan et al. (2017). NAGAP images were supplemented by aerial imagery collected by the National Park Service in 2005 and by the US Geological Survey prior to 1967.

Additional topographic data come from aerial lidar datasets collected between 2002 and 2012, including a complete survey of Mount Rainier National Park collected in 2007 and 2008. All areas of interest for this study were part of the 2008 data collection, and so this dataset is referred to as the 2008 lidar throughout. Finally, topography of all four study basins was derived from Maxar/DigitalGlobe WorldView-1 stereo satellite imagery acquired on 8 August 2017 (Menounos et al., 2019; Shean et al., 2016).

Aerial imagery was scanned from negatives or diapositives at resolutions of between 14 and 25 μm. One exception was the 1960 imagery around the South Tahoma Glacier, where print images were

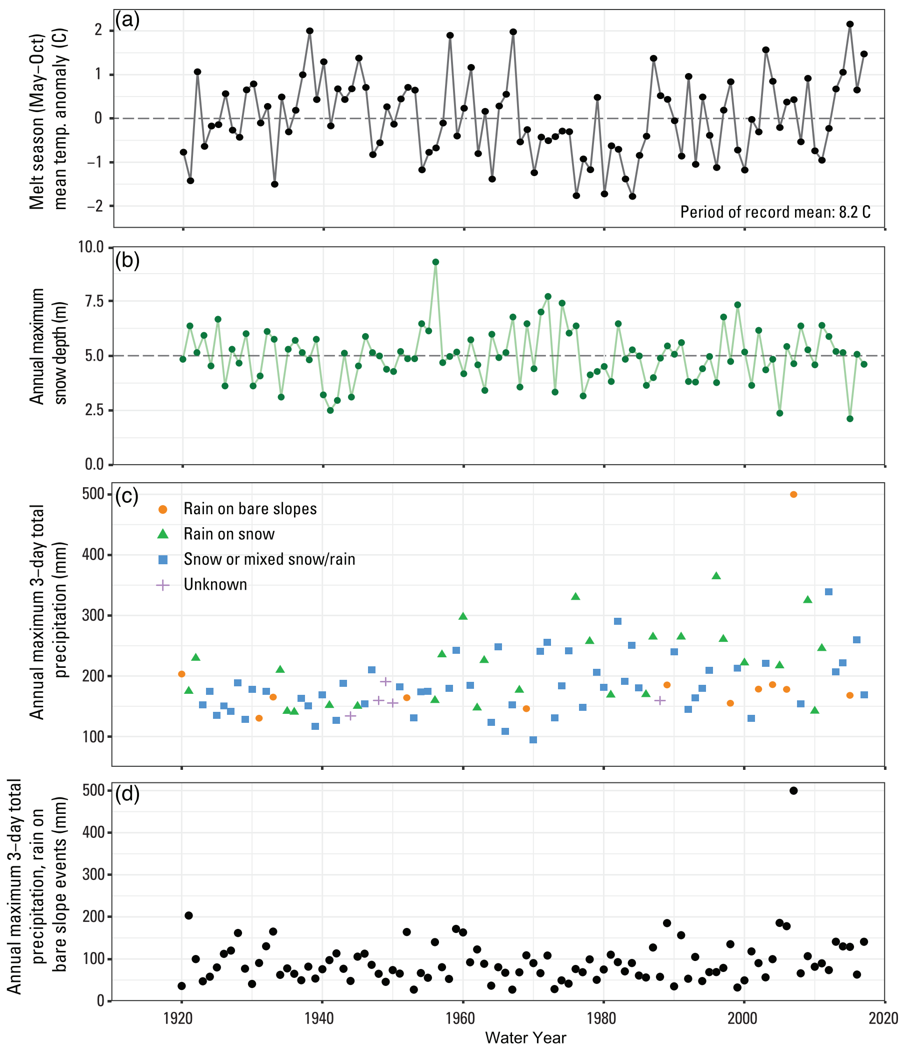

FIGURE 3 Summarized climatic data from the Rainier Paradise Ranger Station (Figure 1; NOAA GHCND:USC00456898). (a) Mean temperature anomalies over the summer melt season (May to October). (b) Annual maximum snow depth. (c) Annual maximum 3-day total precipitation. Events are classified based on mean temperature over the event and the recorded snow pack depth. (d) Annual maximum 3-day total precipitation for events where rain fell on bare slopes

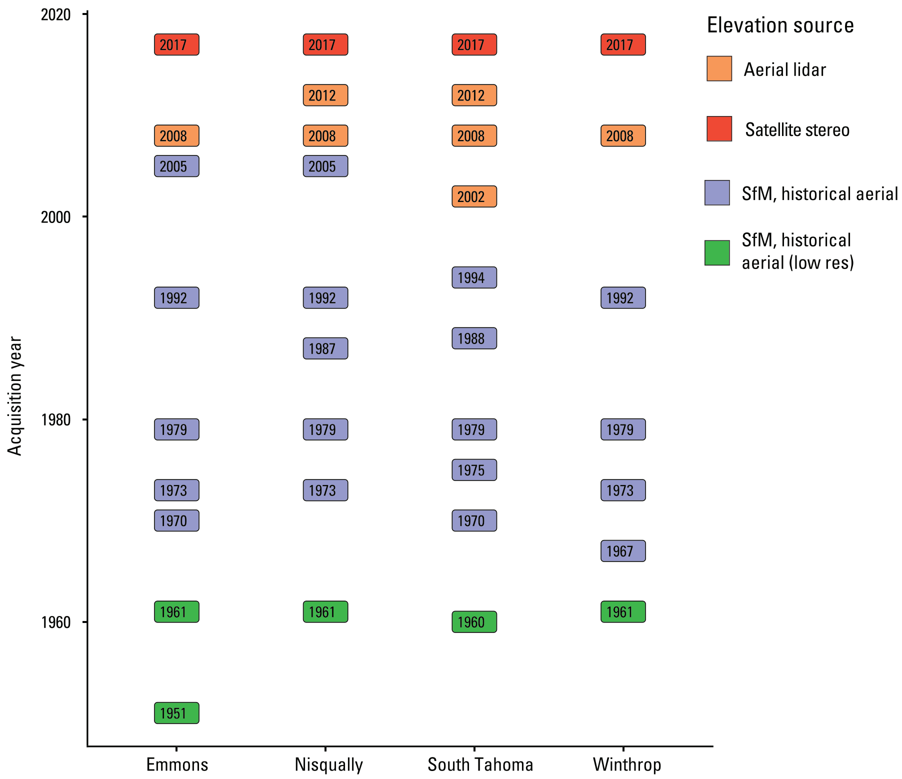

FIGURE 4 Summary of digital elevation models used in this study

TABLE 2 Sources of topography used in this study

Watershed	Year	Topography source	Imagery resolution (μm)	Ground resolution (m)	DEM posting (m)	Source data repository
Emmons	1951	Aerial imagery	25.4	0.66	2.0	https://earthexplorer.usgs.gov/
	1961	Aerial imagery	25.4	0.65	2.0	https://earthexplorer.usgs.gov/
	1970	Aerial imagery	20.0	0.20	0.5	Nolan et al., 2017 https://doi.org/10.18739/A2VH5CJ8K.
	1973	Aerial imagery	20.0	0.19	0.5	Nolan et al., 2017 https://doi.org/10.18739/A2VH5CJ8K.
	1979	Aerial imagery	20.0	0.33	1.0	Nolan et al., 2017 https://doi.org/10.18739/A2VH5CJ8K.
	1987	Aerial imagery	20.0	0.19	0.5	Nolan et al., 2017 https://doi.org/10.18739/A2VH5CJ8K.
	1992	Aerial imagery	20.0	0.26	1.0	Nolan et al., 2017 https://doi.org/10.18739/A2VH5CJ8K.
	2005	Aerial imagery	14.0	0.22	0.5	Anderson, 2021 https://doi.org/10.5066/P9056ZNG
	2008	Lidar	–	–	1.0	https://lidarportal.dnr.wa.gov/
	2017	Maxar/Digital Globe imagery	8.0	0.50	2.0	Source imagery not publicly available
Nisqually	1961	Aerial imagery	25.4	0.78	2.0	https://earthexplorer.usgs.gov/
	1973	Aerial imagery	20.0	0.21	1.0	Nolan et al., 2017 https://doi.org/10.18739/A2VH5CJ8K.
	1979	Aerial imagery	20.0	0.18	0.5	Nolan et al., 2017 https://doi.org/10.18739/A2VH5CJ8K
	1987	Aerial imagery	20.0	0.19	0.5	Nolan et al., 2017 https://doi.org/10.18739/A2VH5CJ8K
	1992	Aerial imagery	20.0	0.22	0.5	Nolan et al., 2017 https://doi.org/10.18739/A2VH5CJ8K
	2005	Aerial imagery	14.0	0.40	1.0	Anderson 2021 https://doi.org/10.5066/P9056ZNG
	2008	Lidar	–	–	1.0	https://lidarportal.dnr.wa.gov/

(Continues)

TABLE 2 (Continued)

Watershed	Year	Topography source	Imagery resolution (μm)	Ground resolution (m)	DEM posting (m)	Source data repository
	2012	Lidar	–	–	1.0	https://lidarportal.dnr.wa.gov/
	2017	Maxar/Digital Globe imagery	8.0	0.50	2.0	Source imagery not publicly available
South Tahoma	1960	Aerial imagery	42.3	0.81	2.0	Anderson 2021 https://doi.org/10.5066/P9056ZNG
	1970	Aerial imagery	20.0	0.19	0.5	Nolan et al., 2017 https://doi.org/10.18739/A2VH5CJ8K
	1975	Aerial imagery	20.0	0.19	0.5	Nolan et al., 2017 https://doi.org/10.18739/A2VH5CJ8K
	1979	Aerial imagery	20.0	0.18	0.5	Nolan et al., 2017 https://doi.org/10.18739/A2VH5CJ8K
	1988	Aerial imagery	20.0	0.33	1.0	Nolan et al., 2017 https://doi.org/10.18739/A2VH5CJ8K
	1994	Aerial imagery	20.0	0.09	0.5	Nolan et al., 2017 https://doi.org/10.18739/A2VH5CJ8K
	2002	Lidar	–	–	2.0	https://lidarportal.dnr.wa.gov/
	2008	Lidar	–	–	1.0	https://lidarportal.dnr.wa.gov/
	2012	Lidar	–	–	1.0	https://lidarportal.dnr.wa.gov/
	2017	Maxar/Digital Globe imagery	8.0	0.50	2.0	Source imagery not publicly available
Winthrop	1951	Aerial imagery	25.4	0.66	2.0	https://earthexplorer.usgs.gov/
	1961	Aerial imagery	25.4	0.65	2.0	https://earthexplorer.usgs.gov/
	1967	Aerial imagery	20.0	0.28	1.0	Nolan et al., 2017 https://doi.org/10.18739/A2VH5CJ8K
	1973	Aerial imagery	20.0	0.20	0.5	Nolan et al., 2017 https://doi.org/10.18739/A2VH5CJ8K
	1979	Aerial imagery	20.0	0.33	1.0	Nolan et al., 2017 https://doi.org/10.18739/A2VH5CJ8K
	1992	Aerial imagery	20.0	0.26	1.0	Nolan et al., 2017 https://doi.org/10.18739/A2VH5CJ8K
	2008	Lidar	–	–	1.0	https://lidarportal.dnr.wa.gov/
	2017	Maxar/Digital Globe imagery	8.0	0.50	2.0	Source imagery not publicly available

scanned at 42 μm. Photogrammetric processing was done using Agisoft Photoscan Pro (version 1.4.3); processing summaries for all DEMs are available at Anderson (2021). Ground control points were manually identified using 0.5 m lidar intensity images from the 2008 lidar, with corresponding elevations obtained from the 2008 bare earth DEM. Ground control points were selected to be distinct, persistent, and low-lying features in low-relief parts of the landscape visible in both the historical aerial imagery and lidar intensity images. These points tended to be distinct rocks in areas of vegetation or low vegetation in areas of otherwise bare sediment. The 8 August 8 2017 stereo DEM was generated from 0.5 m WorldView-1 images using the NASA Ames Stereo Pipeline (ASP Beyer et al., 2018; Shean et al., 2016) following the methods outlined in Shean et al. (2016).

In order to reduce relative vertical and horizontal offsets, each DEM was co-registered to the 2008 lidar. Co-registration was accomplished by identifying patches of the landscape where both measured change and landscape context indicate that they remained stable over the relevant time interval. Systematic vertical and horizontal offsets were reduced based on relations between slope, aspect, and measured change in these stable areas (Nuth & Kääb, 2011). For all SfM-derived DEMs, residual nonlinear "doming" errors (James & Robson, 2014) were further reduced by fitting a surface to the residual elevation errors over the stable patches. Interpolation was done using diffusion interpolation with a 500 m bandwidth (Esri, 2020). The interpolated error surface was then subtracted from the DEM to obtain a final corrected product.

3.2 | Analysis of geomorphic change

For each study basin, sequential DEMs were subtracted to create DEMs of difference (DoDs). Areas of geomorphic change within the proglacial limits attributable to the movement of sediment were visually identified and delineated. Areas where the ablation of ice was judged likely to be intermixed with the signature of sediment movement were not included in the analysis. Gross erosion, gross deposition, and net change were then calculated over these delineated areas of interest. Estimates of gross erosion and gross deposition were calculated after first thresholding DoDs at the 90% confidence interval

(CI) level (methods for estimating DoD error parameters are described below); estimates of net change were based on unthresholded DoDs (Anderson, 2019).

Several DoDs provided partial or complete coverage over valley floor settings immediately downstream of the proglacial areas. Change was typically dominated by deposition linked to concurrent erosion in proglacial areas. In these cases, downvalley geomorphic change was quantified separately from change above the proglacial limits.

This work was motivated by an interest in how rates of bed material export past the proglacial limits have varied over time. The study methods used here provide estimates of subaerial erosion, which we presume is a major control on that export rate. However, the actual bed material flux passing the proglacial limits also includes material sourced from subglacial, supraglacial, or glacier marginal settings, where we cannot isolate sediment transfers using repeat topography. Conversely, some fraction of the subaerial erosion we can measure will involve fine material, and so not part of the bed material load. Within the results below, we focus on documenting and discussing the volumetric erosion and export of sediment we can see, independent of any assumption about grain size distribution or the potential for additional sediment delivery from glacier-masked areas. We then consider in the discussion how closely that erosion may approximate total variations in bed material export.

3.2.1 | Estimating uncertainty

An error analysis of the DoDs was conducted based on measured change in stable parts of the landscape. Stable areas were manually identified in each DoD; these polygons were created independently from the polygons used for the co-registration analysis, though areas used in the co-registration procedures were not explicitly excluded. For a given DoD, many distinct stable areas were delineated, spread across the study area and with total areas similar to typical areas of the change analysis.

Mean errors were generally $\pm$0.20 m (Table 3). Measurement precision, defined as half the 5th to 95th percentile range of individual measurements, was lowest for the DoDs based on aerial lidar pairs (about $\pm$0.20 m) and highest for DoDs involving 1960s imagery (around $\pm$2 m). Precision for the remaining products ranged from $\pm$0.5 to $\pm$1.5 m.

The spatial correlation of random errors was assessed using semivariogram analysis, after first downsampling all DoDs to a 10 m grid using simple area-averaging. This downsampling averages out random noise with short correlation ranges, which tends to largely cancel out when propagated (Anderson, 2019), while allowing us to efficiently identify longer-range correlation structures that do contribute meaningful uncertainty. Empirical semivariograms were fit using a spherical semivariogram model with no nugget (Rolstad et al., 2009). Estimated semivariogram range values were generally between 30 and 60 m, but occasionally extended up to 100 m.

Uncertainty in estimated volumetric change was quantified using an error model that included both a spatially correlated random error component and an uncorrected systematic offset. Correlated error range and magnitudes were estimated for each DoD based on fitted semivariogram models described above (Table 3). The potential uncorrected systematic error was assumed to be $\pm$0.20 m in all cases, reflecting the range of observed mean errors. Error was propagated according to statistical methods described in Rolstad et al. (2009) and Anderson (2019). Uncertainties were generally small (<20%) in comparison to the magnitude of observed geomorphic change. In practical terms, limited information about grain size distributions and the obscuring or conflation of sediment transfers by ice are probably more important than survey imperfection in terms of our ability to interpret results.

3.3 | Landsat analysis

At Mount Rainier, major debris flows and floods clear large swathes of vegetation growing in river valleys, while dense alder thickets tend to rapidly recolonize stable gravel surfaces. Annual normalized difference vegetation index (NDVI) images derived from 30 m Landsat surface reflectance data provide information about the changing extents of vegetation cover over time and have been used to refine the timing of significant geomorphic events since 1984.

All NDVI products were obtained using the Climate Engine interface (Huntington et al., 2016). For each year, the Climate Engine was used to obtain a composite NDVI image averaging all Landsat-derived NDVI products collected between 15 July and 15 September. This period was selected to encompass when valley floor vegetation is typically green and clearly distinguishable from bare sediment. Separate annual images were created from Landsat 5 and 7 satellites for years with overlapping collections. In the period of overlap, Landsat 7 estimates of mean NDVI were found to be systematically higher than estimates from Landsat 5 by 0.03. All Landsat 7 estimates where then shifted down by this amount to create a consistent record across the satellites.

Change over time was quantified in terms of the mean NDVI value calculated over fixed areas of interest within valley floors, generally downvalley of proglacial areas (Figure 1). The downvalley extents of these areas were selected to cover areas of deposition and/or disturbance associated with major proglacial debris flows, while the cross-valley extents included all Landsat pixels that were vegetation free (defined as an NDVI value of less than 0.3) at any point between 1984 and 2017. In the West Fork White River adjacent to the Winthrop Glacier, two separate areas of interest were delineated: a smaller upper area of interest, where geomorphic activity prior to 2006 is detectable; and a larger downstream area that covers the full scope of changes following the 2006 event.

3.4 | Longitudinal profiles of valley floors

Longitudinal profiles of the primary valley floors were extracted from all DEMs with complete coverage of the proglacial valley floor. When available, these profiles were also extended down the first kilometer below the proglacial limits. For each basin, a single static valley centerline was digitized and used to define regular perpendicular cross-sections. For each DEM, the minimum elevation along each cross-section was used to define the elevation at that distance. Distances were referenced so that zero represents the location of the 19th-century glacial maxima.

TABLE 3 Error analysis and volumetric change for all DoDs

Site	Start year	End year	DEM sources[a]	Interval (yrs)	DoD cell size (m)	Mean error (m)	Correlated error (95% CI, m)	Correlation range (m)
Emmons	1961	1970	AI-AI	9	2	−0.08	2.54	64
	1970	1973	AI–AI	3	0.5	−0.01	0.39	32
	1973	1979	AI–AI	6	1	0.17	0.65	37
	1979	1992	AI–AI	13	1	−0.18	0.58	33
	1992	2005	AI–AI	13	1	0.17	0.41	61
	2005	2008	AI–Lidar	3	1	−0.04	0.37	63
	2008	2017	Lidar–WV	9	2	−0.12	0.34	25
	1961	2008	AI–Lidar	47	2	–	0.74	60
Nisqually	1961	1973	AI–AI	12	2	0.10	1.73	55
	1973	1979	AI–AI	6	1	−0.19	0.72	38
	1979	1992	AI–AI	13	0.5	−0.16	0.74	60
	1992	2005	AI–AI	13	1	0.05	0.56	59
	2005	2008	AI–Lidar	3	1	0.01	0.45	37
	2008	2012	Lidar–Lidar	4	1	0.03	0.13	24
	2012	2017	Lidar–WV	5	2	0.11	0.60	35
	2005	2008	AI–Lidar	3	1	–	0.45	37
South Tahoma	1960	1970	AI–AI	10	2	−0.22	2.93	61
	1970	1975	AI–AI	5	0.5	−0.04	0.56	115
	1975	1979	AI–AI	4	0.5	0.01	0.62	107
	1979	1988	AI–AI	9	1	−0.10	0.59	78
	1988	1994	AI–AI	6	1	0.01	0.51	51
	1994	2002	AI–Lidar	8	1	−0.02	0.52	57
	2002	2008	Lidar–Lidar	6	1	−0.05	0.23	21
	2008	2012	Lidar–Lidar	4	1	0.05	0.18	22
	2012	2017	Lidar–WV	5	2	−0.34	0.42	22
	1988	2002	AI–Lidar	14	1	–	0.74	60
Winthrop	1961	1967	AI–AI	6	2	−0.06	1.24	30
	1967	1973	AI–AI	6	1	−0.01	0.58	61
	1973	1979	AI–AI	6	1	0.22	0.98	28
	1979	1992	AI–AI	13	1	−0.28	1.05	31
	1979	2008	AI–Lidar	29	1	–	0.74	60
	1992	2008	AI–Lidar	16	1	−0.05	0.39	30
	2008	2017	Lidar–WV	9	2	−0.23	0.42	33
	1979	2008	AI–Lidar	29	1	–	0.74	60

[a]AI, aerial imagery; WV, Worldview Imagery.
[b]Blue entries indicate significant net erosion; red entries indicate significant net deposition; black italics indicate non-significant net change.

TABLE 3 (Continued)

Site	DoD precision (90% CI, m)	Unthresholded AOI (m^2)	Net change (m^3)[b]	Gross erosion (m^3)	Gross deposition (m^3)	Note
Emmons	1.89	181,000	965,000 ± 91,000	−128,000 ± 9,000	1,087,000 ± 77,000	Deposition from ’63 rockfall; incomplete
	0.52	90,000	−45,000 ± 21,000	−97,000 ± 7,000	50,000 ± 10,000	
	0.88	169,000	−59,000 ± 42,000	−228,000 ± 15,000	166,000 ± 15,000	
	0.69	233,000	−230,000 ± 54,000	−280,000 ± 24,000	50,000 ± 10,000	
	0.45	454,000	−164,000 ± 104,000	−492,000 ± 35,000	324,000 ± 40,000	
	0.41	340,000	*6,000 ± 79,000*	−141,000 ± 23,000	151,000 ± 25,000	
	0.49	315,000	*56,000 ± 67,000*	−81,000 ± 13,000	133,000 ± 26,000	
	–	145,000	−10,510,000 ± 42,000	−10,514,000 ± 42,000	1,000 ± 1,000	AOI is solely rockfall source area
Nisqually	1.44	208,000	*−51,000 ± 76,000*	−491,000 ± 29,000	441,000 ± 40,000	
	0.90	111,000	−151,000 ± 29,000	−188,000 ± 13,000	41,000 ± 7,000	
	1.00	183,000	*−39,000 ± 52,000*	−170,000 ± 21,000	134,000 ± 20,000	
	0.63	267,000	*−53,000 ± 67,000*	−204,000 ± 21,000	146,000 ± 24,000	
	0.53	544,000	−882,000 ± 119,000	−1,031,000 ± 58,000	150,000 ± 22,000	
	0.21	309,000	*−8,000 ± 63,000*	−103,000 ± 15,000	92,000 ± 24,000	
	0.68	111,000	*26,000 ± 28,000*	−36,000 ± 5,000	56,000 ± 11,000	
	0.53	94,000	242,000 ± 23,000	−9,000 ± 1,000	251,000 ± 20,000	Deposition beyond proglacial extents
South Tahoma	2.13	36,000	−257,000 ± 34,000	−256,000 ± 29,000	1,000 ± 2,000	
	0.42	96,000	−478,000 ± 35,000	−493,000 ± 29,000	16,000 ± 5,000	
	0.53	105,000	−215,000 ± 38,000	−242,000 ± 21,000	25,000 ± 10,000	
	0.56	100,000	−814,000 ± 32,000	-826,000 ± 26,000	13,000 ± 4,000	
	0.63	261,000	−2,077,000 ± 63,000	−2,135,000 ± 47,000	61,000 ± 8,000	
	0.59	429,000	−970,000 ± 101,000	−1,123,000 ± 61,000	156,000 ± 21,000	
	0.32	645,000	−2,215,000 ± 132,000	−2,310,000 ± 87,000	96,000 ± 15,000	
	0.18	525,000	−270,000 ± 107,000	−468,000 ± 44,000	196,000 ± 38,000	
	0.54	552,000	−643,000 ± 116,000	−736,000 ± 64,000	110,000 ± 15,000	
	1.00	648,000	1,972,000 ± 158,000	−195,000 ± 12,000	2,163,000 ± 139,000	Deposition beyond proglacial extents
Winthrop	1.50	1,230	*30 ± 1,290*	−50 ± 30	330 ± 400	
	0.72	37,000	*−5,000 ± 13,000*	−15,000 ± 4,000	10,000 ± 4,000	
	0.98	14,000	*9,000 ± 6,000*	−1,000 ± 0	8,000 ± 2,000	
	1.05	72,000	−112,000 ± 21,000	−141,000 ± 9,000	30,000 ± 5,000	
	1.00	68,000	−306,000 ± 23,000	−312,000 ± 20,000	7,000 ± 3,000	AOI is erosion associated with 2006 storm that occurred outside the extents of the ’92–’08 DoD
	0.50	416,000	−1,894,000 ± 89,000	−1,936,000 ± 62,000	47,000 ± 8,000	
	0.52	252,000	*6,000 ± 56,000*	−153,000 ± 18,000	159,000 ± 22,000	
	1.00	41,000	141,000 ± 15,000	−5,000 ± 1,000	146,000 ± 14,000	Deposition beyond proglacial extents

4 | RESULTS

4.1 | Nisqually Glacier

In the proglacial zone below the Nisqually Glacier, erosion associated with the 2006 storm accounts for nearly all measurable net erosion since 1961 (Figure 5 and Table 3), and the most pronounced single-year clearing of vegetation from downvalley debris flow depositional zones (Figure 6).

Erosion associated with the 2006 storm initiated where runoff from unglaciated slopes to the east fell steeply into the glacial valley (Figure 7c-i; roman numerals are used to indicate the location of specific features in figures). The routing and entry of runoff were governed by the geometry of a downstream tapering moraine ridge. Erosion continued along a swath of the valley floor for about 2 km, augmented by two broad failures of morainal material from the east (Figure 7c-ii). Surface lowering was about 3–10 m in the eroding valley floor, and 10–20 m in the moraine failures. Post-2006 aerial imagery shows that the channel scoured to bedrock in several parts of the valley floor.

Mobilized material began to deposit downvalley of the second slope failure, filling the full width of the valley floor 2–4 m deep. Deposition extended beyond the downvalley limits of the DoD. Over the extent of available data, valley floor deposition totaled 240,000 ± 20,000 m^3, representing about a quarter of the 1,030,000 ± 60,000 m^3 eroded upvalley. Deposited material largely remained in storage through 2017 (Figure 7d).

In the decades prior to 2006, geomorphic activity primarily occurred along the valley floor and the eastern margin of the valley (Figure 7a,b). This activity included a zone of persistent slope failure lower in the valley (Figure 7a-iii,b-iii) and several distinct hollow-like features in moraine slopes (Figure 7a-iv,b-iv). Mobilized material accumulated near the toe of the valley wall and/or along the glacial margin. Change in the valley floor over the earlier intervals included both significant net erosion and net deposition. Deposition was not connected to any distinct upvalley source, and may have been sourced from subglacial or glacier-marginal sediments.

4.2 | South Tahoma Glacier

The proglacial zone below the South Tahoma Glacier has experienced persistent erosion since 1960 associated with the incision of a gully-like channel (Figure 8). As of 2017, this channel was about 50–80 m

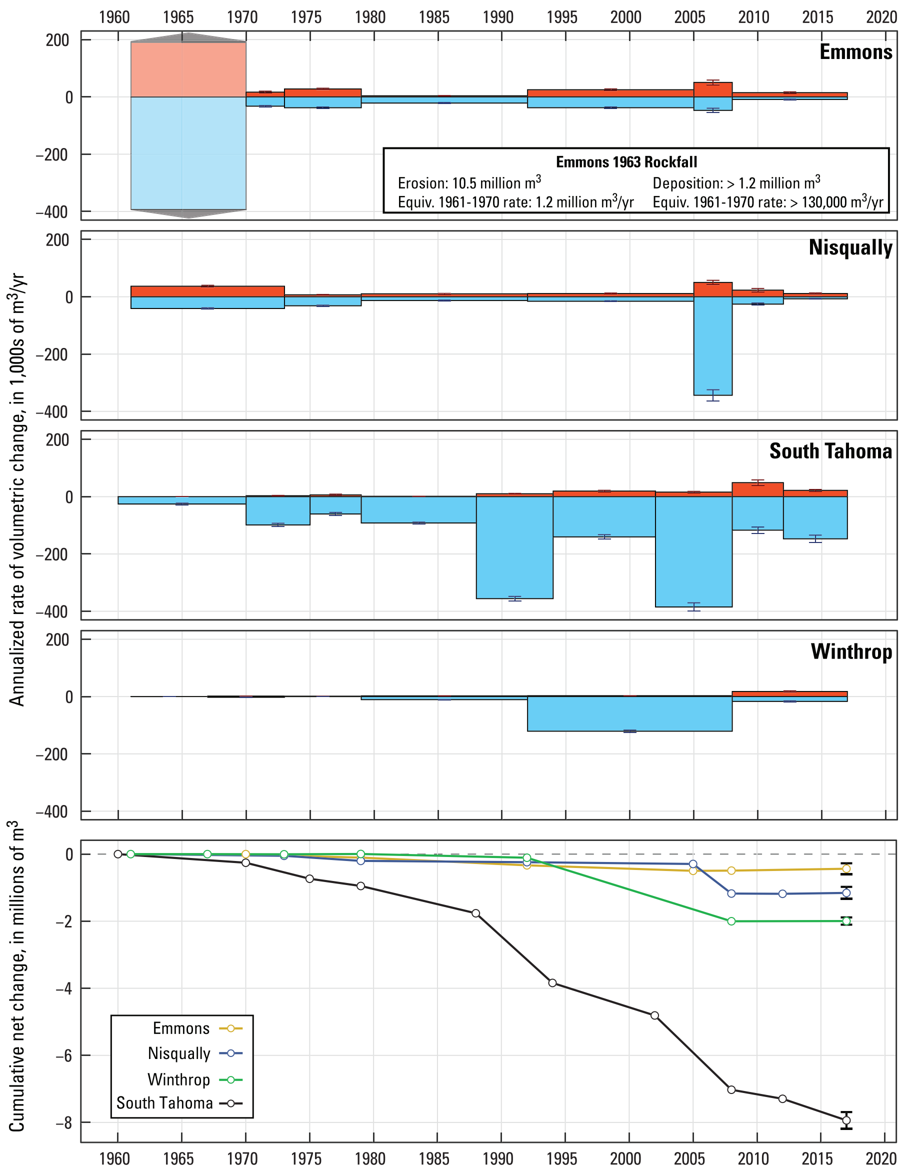

FIGURE 5 Gross erosion and deposition, converted to an effective annual rate, for (a) the Emmons Glacier proglacial zone, (b) the Nisqually Glacier proglacial zone, (c) the South Tahoma Glacier proglacial zone, and (d) the Winthrop Glacier proglacial zone. (e) Cumulative net change for the four study basins. In the Emmons, the cumulative net change was started in 1970, excluding 1963 rockfall impacts

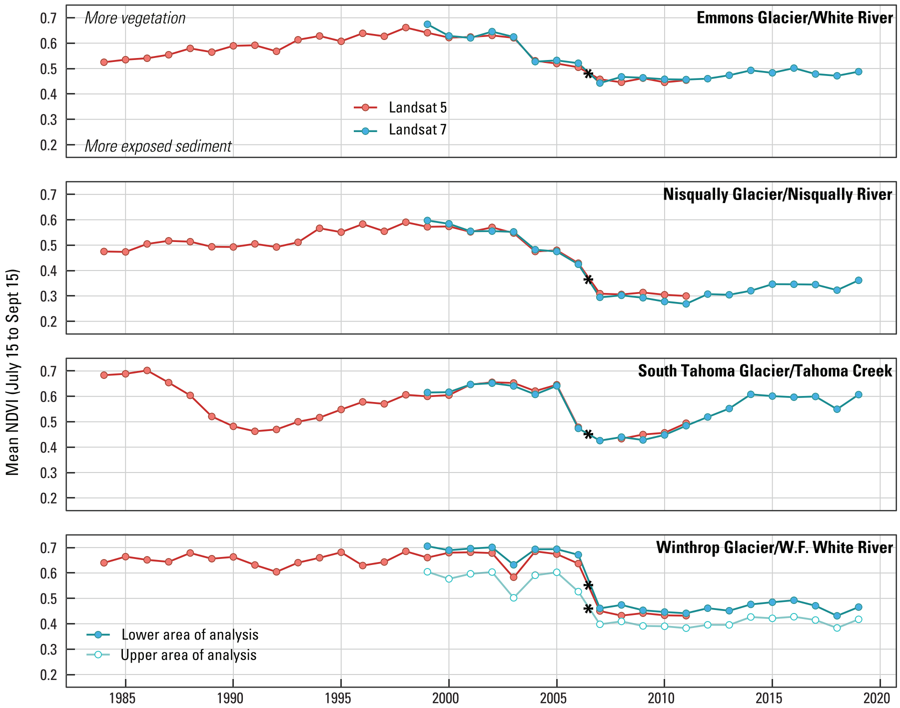

FIGURE 6 Time series of mean normalized difference vegetation index (NDVI) values based on 15 July to 15 September Landsat imagery. Higher values indicate more vegetation; lower values indicate more bare sediment. Spatial extents of averaging are shown in Figure 1. Asterisk indicates interval showing impacts of the 2006 storm

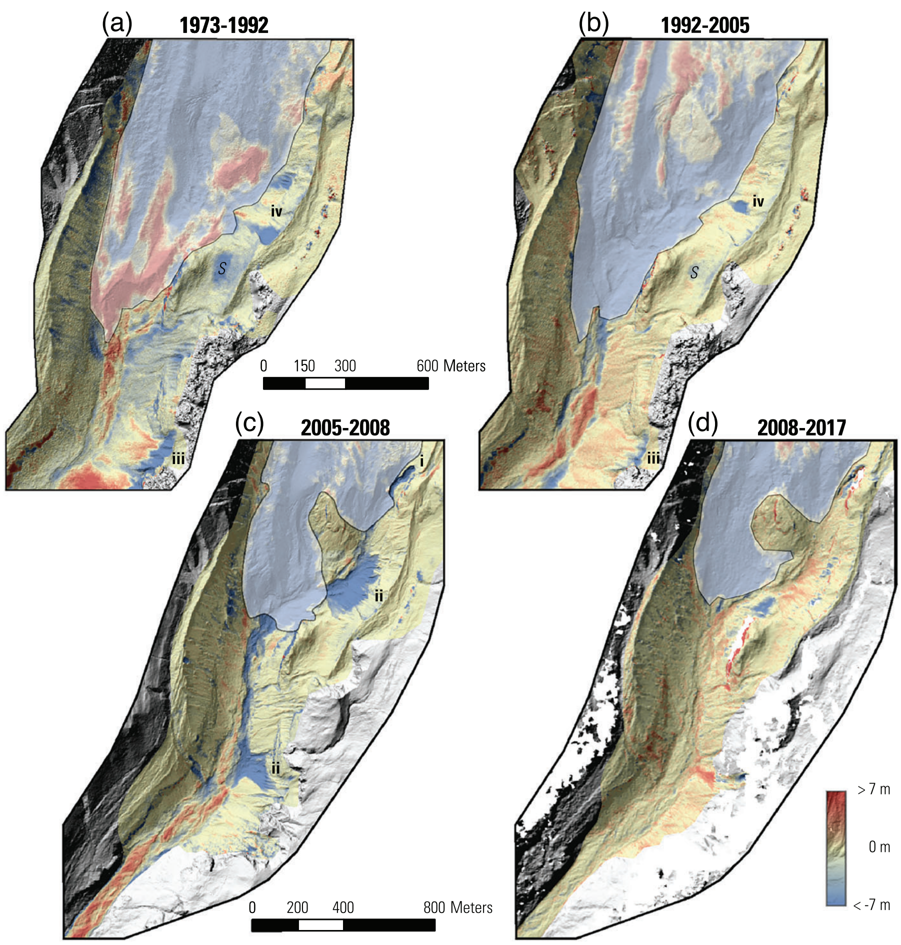

FIGURE 7 DoDs showing elevation changes in the Nisqually Glacier proglacial area from (a) 1973 to 1992, (b) 1992 to 2005, (c) 2005 to 2008, and (d) 2008 to 2017. Opaque polygons indicate where elevation changes are partly or wholly the result of changes in the extent or elevation of the Nisqually Glacier. Surface lowering likely associated with melting of disconnected stagnant ice is denoted by the letter S. Roman numerals are used to notate features referenced in the text, ordered by their appearance in the text. Note that extent and scale of A and B are different than for C and D

deep and 2 km long. The nascent eroding channel is visible in 1961 imagery and topography but not in 1940s ground-based imagery, bracketing the onset of its formation. Erosion rates have been an order of magnitude higher than the other three basins, and it is the only basin in which detectable net erosion occurred in all DoD intervals (Figure 5 and Table 3). Much of the erosion has been associated with debris flows triggered by summer or early fall outburst floods (Walder & Driedger, 1995).

Erosion rates in the South Tahoma Glacier proglacial area were notably higher than average during the 1988–94 and 2002–08 intervals (Figure 5). Higher erosion rates from 1988–94 correspond to a well-documented period of outburst flood activity associated with

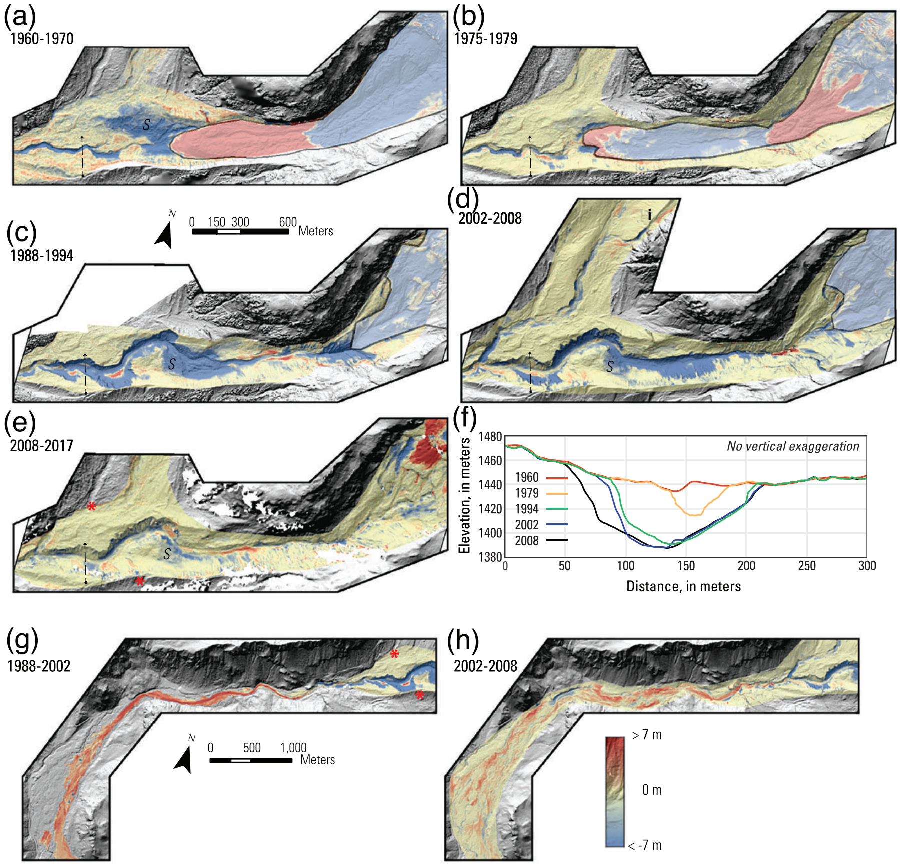

FIGURE 8 DoDs showing elevation change in the South Tahoma Glacier proglacial zone from (a) 1960 to 1970, (b) 1975 to 1979, (c) 1988 to 1994, (d) 2002 to 2008, and (e) 2008 to 2017. (f) Repeat cross-sections cut from DEMs, showing progressive incision of the valley floor. Location of the cross-section shows as dashed line in A–E. (g) DoD showing downstream deposition from 1988 to 2002 and (h) from 2002 to 2008. Opaque polygons indicate where elevation changes are partly or wholly the result of changes in the extent or elevation of the South Tahoma Glacier. Surface lowering likely associated with melting of disconnected stagnant ice is denoted by the letter S. Roman numerals are used to notate features referenced in the text, ordered by their appearance in the text. Red asterisks in (e) and (g) indicate coincident points between the two extents

warm summers (Figure 3) and the stagnation and rapid retreat of the terminus of the South Tahoma Glacier (Walder & Driedger, 1994). High erosion rates over the 2002–08 period are partly attributable to the 2006 storm; however, the basin also experienced a large outburst flood/debris flow in the summer of 2005. That 2005 event was responsible for most of the loss of downstream valley floor vegetation over this period (Figure 6). The extent of vegetation removal indicates that the 2005 debris flow was large and likely contributed to elevated net erosion over the 2002–08 interval.

Over the past half-century, material eroded from the proglacial area has tended to start dropping out immediately downvalley of the 19th-century glacial maxima (Figure 8g,h). Deposition often continued over the next 4–5 km, and repeated debris flows have filled the broad valley floor below the proglacial limits several meters across its width. Over the 2002–08 and 2008–12 intervals, about half of the net erosion from the proglacial zone could be accounted for in these downstream deposits (Anderson & Pitlick, 2014). Measurable deposition from 1988 to 2002 totaled 2.1 ± 0.1 million m^3, representing about two thirds of the 3.0 ± 0.1 million m^3 eroded from the proglacial zone over that same period.

The contributing area of Tahoma Creek at the proglacial limits also includes an area to the north of the primary channel, draining a tongue of the Tahoma Glacier (Figure 2b). That northern channel had initial (1960) valley floor gradients similar to that of the main channel (Supporting Information Figure 1), has experienced identical meteorological forcing and, as a result of the erosion along the main channel, has been subject to a 25 m drop in local base level. Despite these similarities, the valley below the Tahoma Glacier has been markedly less active than the valley below the South Tahoma Glacier. The Tahoma Glacier meltwater channel experienced essentially no detectable geomorphic change outside of the 2006 storm (Figure 8d). Similar to observations in the Nisqually Glacier proglacial zone, erosion during the 2006 event initiated where surface runoff, after funneling along the backside of a tapering moraine ridge, fell into the main valley (Figure 8d-i).

4.3 | Emmons Glacier

From 1961 to 2017, geomorphic activity in the proglacial valley floor below the Emmons Glacier was dominated by deposition from a large rockfall event in 1963. This rockfall originated from a steep promontory rising above the glacier (Figure 9; Crandell and Fahnestock, (1965)). Coupled with the widespread ablation of stagnant ice that filled much of the proglacial valley at the time of the rockfall, the valley floor experienced substantial elevation changes over the 1960–70 DoD interval. However, geomorphic activity in the decades since the rockfall has been modest in comparison to the other basins, and the broad valley floor below the glacier has been predominately depositional (Figures 5 and 10).

From 1970 to 1992, volumetrically modest geomorphic activity occurred along the glacier margins. Activity was most consistent along the western margin, where a meltwater channel regularly undercut the west moraine ridge (Figure 10a-i). After 1992, the most notable geomorphic changes involved the deposition of downstream-tapering wedges of material aligned with the glacier outlet stream. Such deposits were observed over both the 1992–2005 and 2005–08 intervals (Figure 10b-ii,c-ii). Given their geometry, location, and the lack of any obvious upvalley source, these wedges are interpreted as deposits of subglacial sediment entrained during outburst floods.

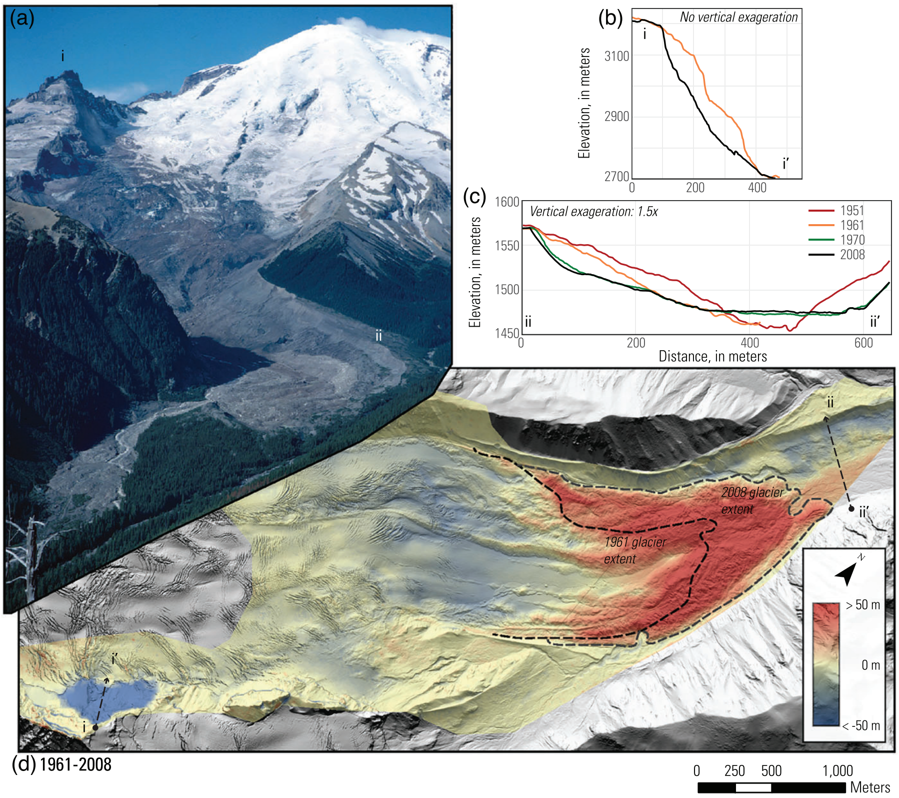

FIGURE 9 Geomorphic impacts of the 1963 rockfall above the Emmons Glacier. (a) Oblique imagery of the Emmons Glacier taken in 1964, showing the source of the rockfall and the distinct light-colored rockfall deposits blanketing the glacier and valley floor. Image source: Dwight Crandell, US Geological Survey Photographic Library, D. R. Crandell Collection, No. 141. (b) Repeat cross-section cut through the source area, based on 1961 and 2008 DEMs. (c) Repeat cross-sections cut through the valley floor; substantial lowering along valley margins from 1951 to 1970 is due to the ablation of stagnant ice. (d) DoD from 1961 to 2008. Roman numerals indicate coincident locations across the panels

Deposition over the 1992–2005 interval is attributed to a single event in 2003, apparent in its impact on downstream vegetation (Figure 6). Deposition over the 2005–08 interval is presumed to be associated with the 2006 storm. Simply based on deposit size, the 2003 event appears to have been the larger event of the two. Geomorphic activity in the watershed from 2008 to 2017 was limited (Figure 10d).

Given that the 2003 and 2006 events were energetic enough to remove vegetation several kilometers downvalley (Figure 6), they were presumably energetic enough to mobilize coarse sediment out of the proglacial zone. However, without any estimate of the initial volume of subglacial erosion, the data here provide no means of estimating that net export.

4.3.1 | The 1963 rockfall

The source area of the 1963 rockfall was visible in 1961–2008 topographic differencing, with local vertical lowering of up to 150 m and a total volumetric loss of 10.50 ± 0.04 million m^3 of material (Figure 9). This estimate of source volume is similar to Crandell and Fahnestock's (1965) estimate of rockfall deposition ($\sim$11 million m^3). This comparison is imperfect, given approximations used in the 1965 estimate of deposition and potential differences in bulk density between source material and deposits. Regardless, the rough similarity in volumes indicates that the deposits mapped by Crandell and Fahnestock (1965) likely represent the large majority of the original source material. The bulk of those deposits came to rest in the broad proglacial valley floor. Additional material was deposited on top of the glacier and a modest volume was transported up to $\sim$500 m beyond the proglacial limits.

Note that the cumulative net change for the Emmons Glacier proglacial zone shown in Figure 5 starts in 1970, excluding impacts of the rockfall. While immense volumes of material were mobilized in this event, most of it appears to have deposited within the proglacial limits, with relatively modest (though unquantified) export of material beyond those limits (Crandell & Fahnestock, 1965). In terms of the sediment budget of just the broad proglacial valley below the Emmons Glacier, this event likely deposited $\sim$7–8 million m^3 of material, with the remaining 3–4 million m^3 emplaced on the glacier or beyond the proglacial limits.

Since 1970, there has been little measurable erosion across the broad proglacial valley floor, indicating that rockfall deposits emplaced in the proglacial valley largely remained in storage through 2017. Rockfall material deposited beyond the proglacial area has experienced some erosion, forming distinct vegetated terraces along the east side of the valley floor. Based on the initial planform extent of these deposits (Figure 9a) and the relative height of those terraces above the active channel measured in the 2008 lidar, we crudely estimate that river erosion has removed about 500,000 m^3 of these downvalley deposits. Taken together, this implies that only a small fraction of the original rockfall source volume has been mobilized down the White River, with most rockfall material having remained in upper valley storage through 2017.

4.4 | Winthrop Glacier

Over the 1961–2017 study period, geomorphic activity in the Winthrop Glacier proglacial area was dominated by erosion during the 2006 storm (Figure 5). Most of that erosion occurred in a series of gully-like channels formed between the western margin of the glacier, several moraines ridges, and the western bedrock valley wall (Figure 11b-i). Although these channels typically drain unglaciated slopes to the west, breaches in the adjacent lateral moraines indicate that glacially sourced water is episodically routed down them.

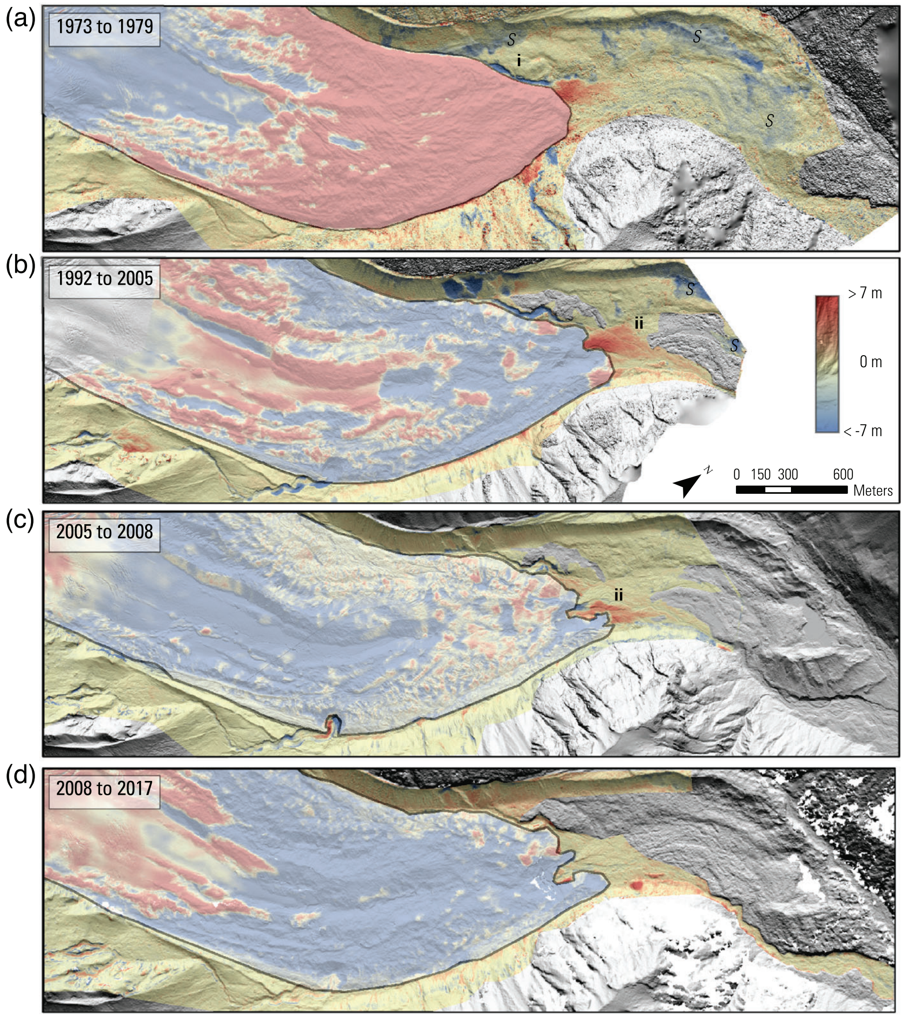

FIGURE 10 DoDs showing elevation change in the Emmons Glacier proglacial zone from (a) 1973 to 1979, (b) 1992 to 2005, (c) 2005 to 2008, and (d) 2008 to 2017. Opaque polygons indicate where elevation changes are partly or wholly the result of changes in the extent or elevation of the Emmons Glacier. Surface lowering likely associated with melting of disconnected stagnant ice is denoted by the letter S. Roman numerals are used to notate features referenced in the text, ordered by their appearance in the text

The 2006 storm deepened and widened the western glacier-marginal channels several meters over a distance of about 4 km, mobilizing at least 2 million m^3 of material. This scour significantly increased the exposure of several bedrock outcrops, which form distinct steps in the channel profile (Figure 12). Mobilized material began to drop out near the confluence of the West Fork White River and Winthrop Creek (the primary outlet stream of the glacier; Figure 11d-ii). Deposition filled the valley floor upwards of 10 m. Distinct young terraces observed in the field in 2017 suggest that meter-scale deposition likely continued to fill the valley floor for at least several kilometers beyond the limits of available data.

While Winthrop Creek experienced measurable geomorphic change during 2006, it was volumetrically minor in comparison to what occurred in the western channels (Figure 11d). The 2006 storm also triggered substantial erosion in several gully-like channels along the eastern margin of the glacier (Figure 11b-iii). However, material mobilized in these channels appears to have been deposited on or under the glacier.

Over the decades preceding the 2006 storm, geomorphic change in the basin was limited. Aerial and Landsat imagery do indicate that a prominent new breach in the left-lateral moraine formed over the 1992–2008 interval (Figure 11b-iv) was the result of a 2005 outburst flood/debris flow, and only enlarged in the 2006 storm. Modest geomorphic change visible in the western channels over the 1979–92 interval (Figure 11a-v) may be related to a 1987 outburst flood noted by Driedger and Fountain (1989).

In the decade since the 2006 storm, geomorphic change has primarily involved lowering along the uppermost parts of sidewall slopes in the western channel, with deposition occurring along the lower flanks of those slopes (Figure 11c-vi). This relaxation of sidewall slopes has not been associated with any measurable net erosion or export of sediment.

4.5 | Valley floor gradients

The gradients of the primary proglacial valley floors, and the change in those gradients over the period of record, vary across the four basins. Of the four, the proglacial area below the South Tahoma Glacier was the steepest in 1960, but that gradient has been steadily dropping over the period of record (Figure 12). This relaxation has progressed in an upstream direction, removing a distinct convexity in the 1960 valley floor. The proglacial area below the Emmons Glacier had the lowest valley floor gradient in 1951—this geometry then pre-dates the 1963 rockfall—but has been slowly steepening as it fills. The gradients of the proglacial valleys below the Nisqually and Winthrop glaciers have changed relatively little since around 1960, and both have gradients of around 0.1 m/m.

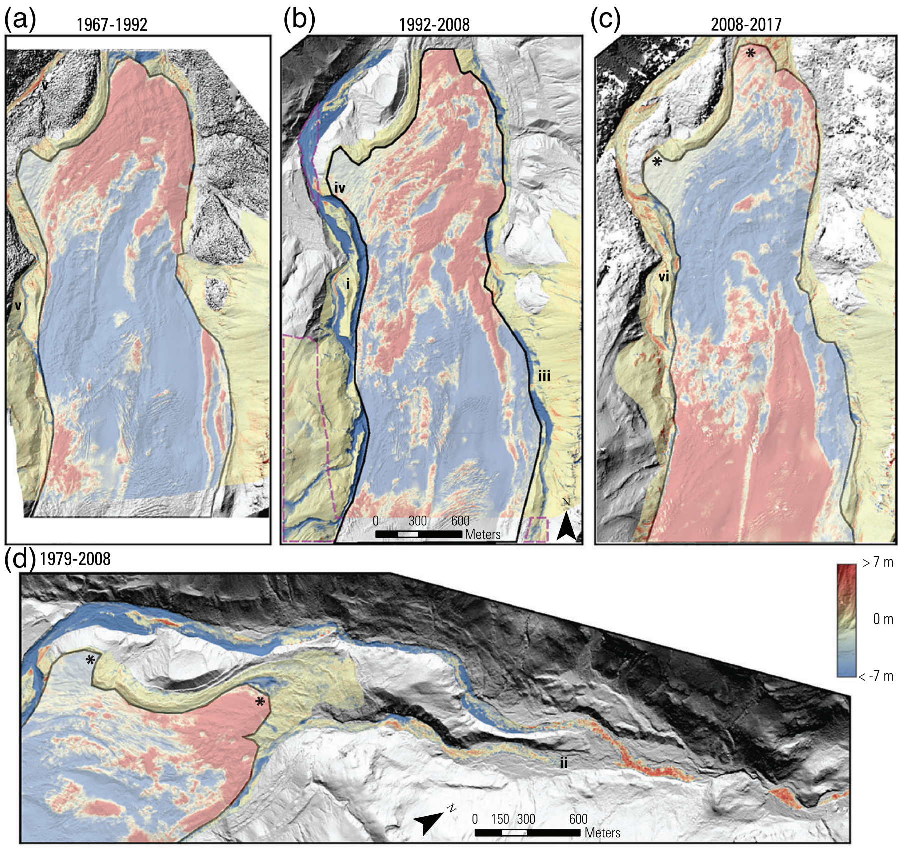

FIGURE 11 DoDs showing geomorphic change in the Winthrop Glacier proglacial zone from (a) 1967 to 1992, (b) 1992 to 2008, and (c) 2008 to 2017. Areas in (b) bounded by purple dashed lines indicate where a 1979–2008 DoD was used to extend the view of 2006 storm impacts. (d) DoD from 1979 to 2008 showing erosion and downstream deposition associated with the 2006 storm. Roman numerals are used to notate features referenced in the text, ordered by their appearance in the text. Black asterisks in (c) and (d) indicate coincident points between the two extents

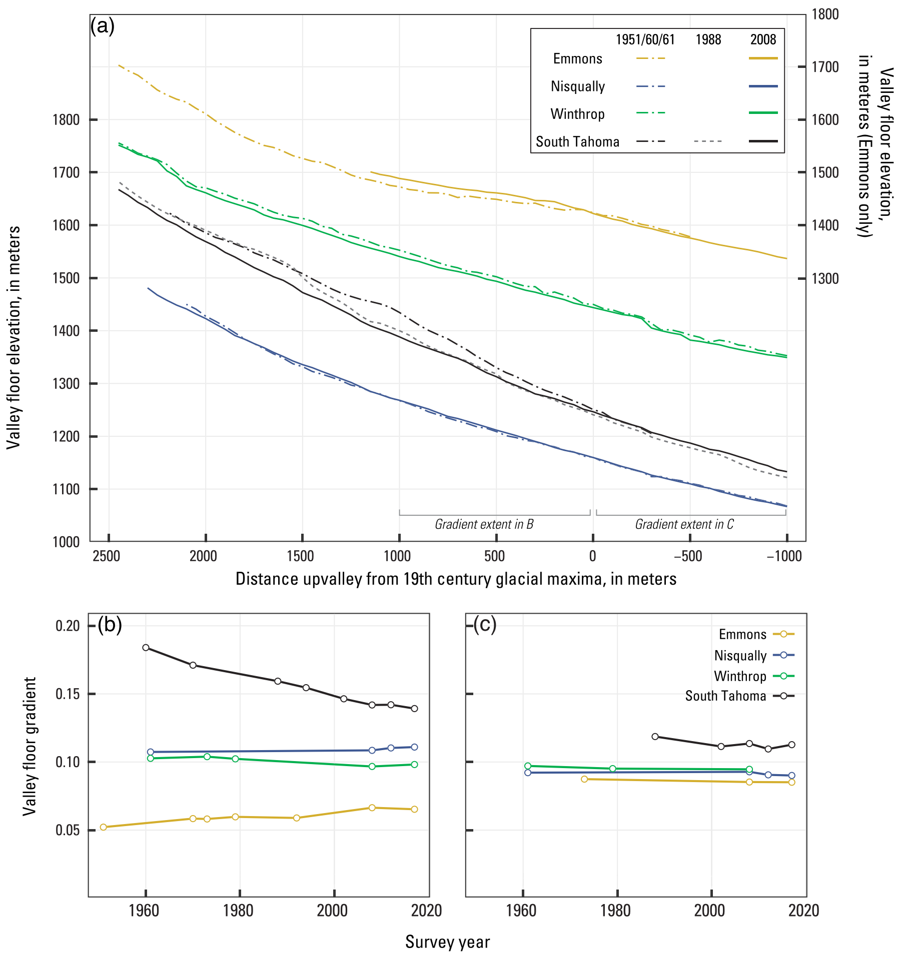

FIGURE 12 (a) Valley long profiles through the proglacial basins. The Emmons profile is plotted against the right axis, which is shifted up 200 m relative to the main axis. (b) Valley gradient over time over the first kilometer upstream of 19th-century maxima. (c) The same as (b), but for the first kilometer downstream of the 19th-century maxima. Profiles for the Winthrop are taken down the West Fork White River (Figure 1)

Immediately downstream of the proglacial limits, the valleys below the Nisqually, Emmons, and Winthrop Glaciers all have similar gradients, and those gradients have not changed markedly since 1961; Tahoma Creek, draining the South Tahoma Glacier, is somewhat steeper than these other three river systems.

5 | DISCUSSION

5.1 | Valley gradient adjustments as a control on recent geomorphic activity

Despite being located around the same stratovolcano, the four basins studied here show substantially different rates and styles of post-1960 geomorphic change. The proglacial zone below the South Tahoma Glacier has seen consistent erosion, steadily exporting relatively large volumes of sediment. The broad proglacial valley below the Emmons Glacier has been acting as a sediment sink and, with the notable exception of the 1963 rockfall, geomorphic activity in the watershed has been modest. The proglacial extents below the Winthrop and Nisqually glaciers both experienced substantial erosion and net sediment export associated with the 2006 storm but have otherwise been relatively inactive (Winthrop) or dominated by internal transfers of hillslope material (Nisqually).

These differences are most readily explained by differences in the initial (c. 1960) gradients of the primary valley floors (Figure 12). To first order, post-1960 geomorphic activity has been defined by the nature of those gradient adjustments. Several factors explain the importance of these valley floor storage trends. First, these valley floors tend to be the largest reservoirs of sediment in these watersheds, as well as the locations where significant channelized runoff is most likely to occur. The storage trends in these valley floors also govern if or when sediment from upslope areas is ultimately mobilized past the proglacial limits. These results add to the body of work pointing to valley geometry and valley floor disequilibrium as a key control on short-term sediment yield response to glacier change (Beylich & Laute, 2015; Cossart, 2008; Meigs et al., 2006; Roussel et al., 2018). In particular, our results highlight the potential for varying valley geometries to result in substantially different responses within a geologically and climatically similar region. These results echo findings by Carrivick and Rushmer (2009), who likewise stressed possible cross-basin variability in proglacial sediment response to climate forcing.

Immediately above the limits of 19th-century glacial maxima, the four valleys in this study appear to have either obtained, or are adjusting towards, a valley floor gradient of about 0.01 m/m (Figure 12b). Given the limited sample size and uncertainty about the ultimate endpoint of the adjusting basins, we are unable to say whether this is meaningful or chance. However, the notion that quasi-equilibrium valley floor gradients are similar across these proglacial basins, and that glacially conditioned deviations from that gradient may help explain or predict variations in postglacial geomorphic adjustments, presents a readily testable hypothesis. We presume that oversteepening would only be important to the degree it occurs in mobile valley fills. In contrast, steep bedrock steps tend to store relatively little sediment and are unlikely to be eroded rapidly once exposed.

Our focus on valley gradient as a control reflects the fact that our study basins encompassed a range of gradients and directions of adjustment. However, glacial material obviously continues to be a potential source of sediment in basins with a quasi-equilibrium valley floor. Our observations in the Nisqually and Winthrop suggest that basins with stable valley floor gradients function somewhat like large debris flow hollows, with episodic flushing events interspersed with periods of relative quiescence.

5.2 | Controls on the timing and location of geomorphic activity

While differences in valley gradient can explain differences in the typical or median rate of sediment export, the specific timing and long-term mean rate of erosion appear to be strongly governed by extreme and/or stochastic events. In our study area, such extreme events include outburst floods, major rain events, or large rockfalls. In contrast, year-to-year rainfall or melt-driven run-off events have accomplished relatively small fractions of the total geomorphic work. Decades with minimal geomorphic activity in a given basin were common. These observations underscore that thresholds for motion in these settings are often high. The sequencing of extreme or relatively rare events is then likely to be a key control on overall erosion and export rates over periods of decades or longer, echoing conclusions drawn by a similar multi-decadal study in proglacial settings (Micheletti & Lane, 2016); Warburton (1990) and Baewert and Morche (2014) have also made similar points, though based on much shorter-term studies. Such extreme events may be important both in terms of the immediate sediment export as well as their ability to breach barrier and increase connectivity moving forward (Cossart et al., 2018). A corollary of these findings is that variations in the median or “typical” hydrological event may have relatively little impact on long-term erosion rates.

High thresholds for motion are also relevant in terms of the specific location of erosion. Excluding the Emmons rockfall, almost all substantial erosion occurred when and where large volumes of water (often contained in debris flows) flowed through a confined zone. Confinement was provided by a mix of bedrock valley walls, moraine ridges, channels incised into fill deposits, and the glacier margins themselves. Conversely, many broad areas of glacial deposits experienced minimal change over the roughly 60-year period of record, including moraines that were not actively undercut by channelized flows.

5.3 | Glacier retreat as a control on recent erosion rates

Glacier retreat is often associated with the onset of a paraglacial period, during which the exposure of unstable glacial sediments and high meltwater discharges are expected to result in relatively high sediment yields (e.g., Antoniazza & Lane, 2021; Ballantyne, 2002a). Sediment yields are generally presumed to subsequently decline as glacial sediment stores are exhausted or stabilized and meltwater discharges decline.

Our study spans a period when glaciers were generally stable or advancing (1960 to roughly 1980) and a period when glaciers were retreating (roughly 1980 to 2017). The exact timing of the transition and actual magnitude of changes in glacier extent differ between the north and south-facing glaciers, with south-facing glaciers having experienced larger variations and transitioning to retreat earlier than north-facing glaciers (Figure 2, Nylen (2004)).

We generally find that recent glacier retreat has not, in and of itself, been a strong predictor of recent erosion rates. We do not see substantial changes in erosion rates coinciding with the onset of retreat, nor do cross-basin differences in the extent of retreat, either since the 1980s or since 19th-century maxima, readily explain cross-basin variations in overall erosion (Figure 5). Instead, variations in erosion rates appear more directly linked to the factors driving the actual export of proglacial material—namely, the occurrence of shear stresses high enough to both initiate motion and induce connectivity to the outlet. Given that shear stress (for channelized flow) is a function of both flow depth and gradient, this explanation encompasses the importance of episodic large water inputs as well as the gradient and confinement of the landscape over which flows travel. Erosion rates then primarily show a punctuated increase between 2003 and 2006, related to the 2006 storm and a series of significant outburst flood/debris flow events that occurred between 2003 and 2005. The high rates of export from the South Tahoma Glacier proglacial area reflect the high shear stresses imparted by regular outburst floods and debris flows moving over a steep and tightly confined valley floor, while the relatively low rates of export from the Emmons Glacier proglacial zone reflect the limited shear stress acting over the low-gradient and unconfined valley floor. The importance of functional connectivity, or lack thereof, in regulating sediment export inferred here continues a well-established trend in recent proglacial sediment studies (Cavalli et al., 2013; Cossart, 2008; Cossart & Fort, 2008; Cossart et al., 2018; Lane et al., 2017; Mancini & Lane, 2020; Micheletti & Lane, 2016; Turley, 2020).

Several prior studies in the region have indirectly assessed the importance of glacier retreat as a control on sediment export through the lens of downstream impacts. Notably, Czuba et al. (2012) found no correlation between active channel width (taken as a proxy for relative bed material transport intensity) and 20th-century glacier retreat in 11 glaciated watersheds around Mount Rainier, including the four studied here. Based on this finding, they inferred a limited role for recent glacier retreat in setting overall rates of bed material delivery. Similarly, in a study of propagating channel elevation changes downstream of a glaciated stratovolcano located ~200 km north of Mount Rainier, Anderson (2019) found that channel elevation trends followed a measure of integrated climate, and not glacier extents, over a period when the two diverged. The results presented in our study here provide direct observational support for the limited role of changing glacier extent inferred in those prior studies.

Several recent studies have explored similar sediment dynamics in the European Alps using multi-decadal repeat topography and unique long-term records of coarse sediment transport (Lane et al., 2017; Micheletti & Lane, 2016). Both studies documented some increasing coarse sediment export associated with warming temperatures, glacier retreat, and increased water yields. However, both ultimately concluded that factors limiting sediment delivery to basin outlets—particularly the limited connection between hillslope and valley floor sediment processes and the rapid depletion of easily mobilized material from newly exposed valley floor sediments—substantially complicated relations between climate and coarse sediment export. Micheletti and Lane (2016), in particular, stress the likely importance of extreme events for inducing connectivity and controlling overall sediment export. The agreement with our results here, at least in terms of variations in coarse sediment export over time, suggests such findings are relevant for proglacial systems across a range of phyiographic settings.

The above discussion is not intended to imply that glacier retreat has no impact on sediment yield, or that the paraglacial concept is not relevant over decadal timescales—recent erosion in our study basins has largely occurred in places that have been exposed by retreat over the past century and a half, and the impact of events like the 2006 storm have presumably been modulated by recent retreat and exposure of sediment. However, glacier retreat does not appear to spontaneously trigger significant erosion and sediment export, and, in cases where retreat exposes low-gradient expanses of valley floor, may limit downvalley sediment export rather than enhance it. Similar to Cossart (2008), we then caution against assuming that glacier retreat over decadal timescales has a strong or consistent effect on watershed-scale coarse sediment export.

Finally, while this work has treated the 1963 rockfall in the Emmons Glacier basin as somewhat distinct from the proglacial processes of primary interest, the volume of material mobilized during that one event was roughly equal to the combined net erosion observed due to all other processes in all four basins over the past 60 years. Most of the source volume from that event was deposited, and has remained, in the broad valley floor below the Emmons Glacier; the impact here was then more a modification of the proglacial valley than a significant delivery of material to downstream river reaches. However, larger events have occurred in the historical record (i.e., the 40 million m^3 1947 Kautz Creek debris flow; Legg et al., (2014)), and lahars occurring over the Holocene have mobilized orders of magnitude more material than any historical events (Crandell, 1971; Scott et al., 1995). The relative importance of such high-magnitude/low-frequency events may be particularly high in proglacial settings on stratovolcanoes. However, there remains an open question as to whether any changes in headwater sediment yield associated with decadal variations climate and/or glacier extent would be significant and discernible in downstream sedimentary records or channel adjustments. It seems likely this will depend at least partly on the local backdrop of disturbances (meteorological, glacial, or mass wasting) that set the long-term tempo of sediment delivery to downstream river systems.

5.4 | Erosion and its relation to total bed material export

This study was motivated by an interest in the potential impacts of proglacial sediment delivery on downstream river channels. To that end, we are ultimately interested in the magnitude and variations in the total flux of coarse material exported past the proglacial limits. How well the subaerial erosion documented here provides a proxy for that total flux depends both on the grain size of the eroded material and the relative importance of subglacial, supraglacial, and glacier-marginal erosion as a concurrent source of coarse sediment.

Mills (1978) found that supraglacial sediment, moraines, and proglacial outwash in multiple basins around Mount Rainier all had relatively similar grain size distributions. Samples typically had median particle diameters between 32 and 128 mm, with material <2 mm in diameter making up 20–35% of the total mass. Those grain size distributions are similar to bed material sampled in multiple rivers high on Mount Rainier (Anderson & Jaeger, 2020; Czuba et al., 2010; Fahnestock, 1963). It is reasonable to then assume that the erosion and export of a cubic meter of proglacial sediment represents the delivery of a sizable fraction of a cubic meter of bed material.

The relative importance of glacier-masked erosion as an unquantified source of bed material is substantially more difficult to constrain. This can be tied to the ongoing difficulty in resolving how much sediment is actively stored subglacially; englacial and supraglacial material may also be significant sources in the glaciers studied here.

Mills (1978) also noted that Tatoosh granodiorite, which underlies many glaciers on Mount Rainier, was relatively abundant in outwash deposits and floodplains of proglacial rivers but nearly absent from moraine and till deposits. This observation generally indicates that these rivers are receiving material ultimately derived from subglacial erosion. However, this does not constrain the sequencing of that export. If subglacial erosion products largely remain in storage until exposed through glacier retreat, and are only subsequently exported in a debris flow, topographic differencing would accurately reflect the export of that material. In contrast, a steady transfer of bed material from subglacials out and through the proglacial zone would go undetected. There is also the possibility that buried ice may make up some fraction of the material entrained in debris flows. While we have attempted to exclude areas where aerial imagery, topography, and patterns of surface elevation change suggest either active or stagnant ice is present, buried ice that melted sufficiently slowly may have gone undetected.

Looking to our own results, the wedges of material deposited in front of the Emmons Glacier terminus in 2003 and 2006 (Figure 10b-ii,c-ii) indicate that coarse sediment stored in, on, or under the glacier can be exported beyond the glacier episodically. However, these deposits were relatively small and unique to the Emmons, making it unclear whether such processes are likely to be significant generally. Conversely, we find the general stability of valley floors between major sediment pulses (Anderson & Jaeger, 2020) difficult to square with there being a substantial (relative to pulse volumes) throughput of bed material carried by typical runoff events.

Ultimately, the two sources of discrepancy between erosion and export considered here remain difficult to constrain quantitatively. Moreover, the two process operate in opposite directions, leaving it unclear whether our reported erosion volumes likely over- or underestimate bed material export. While we suspect that the subaerial erosion documented here is a major component of the integrated coarse sediment export from these watersheds over the study period, direct evidence remains difficult to come by.

5.5 | Deposition and storage of exported sediment

Events that mobilize large volumes of sediment out of the proglacial zone tended to also deposit large volumes of that material along valley floors within several kilometers of the proglacial limits. This observation held true for all four basins, regardless of whether material was mobilized via rockfall, outburst floods, or extreme rainfall. Where upvalley erosion and downvalley deposition were both relatively well constrained (the 1963 rockfall and the South Tahoma Glacier/Tahoma Creek watershed), downvalley deposition could account for between 50% and >90% of the upvalley net erosion.

Once emplaced, these deposits have been remobilized relatively slowly. As of 2017, most material from the 1963 rockfall remained in storage in the upper White River watershed, and valley floor deposits associated with the 2006 storm in all four watersheds have seen fractionally small volumes of reworking over the following decade.

These results suggest that coarse material exported from proglacial zones is not being rapidly mobilized downstream by fluvial transport. Instead, exported material has largely accumulated in valleys immediately below proglacial limits, to be meted out over subsequent decades or centuries. This observation suggests that the downstream river sensitivity to variations in proglacial coarse sediment export is likely to be modulated by storage dynamics through sequential valley floor sediment reservoirs (e.g., Lisle & Church, 2002). The broad valleys linking Mount Rainier to Puget Sound tend to hold extensive volcaniclastic and glacial material accumulated over glacial–interglacial timescales, and this landscape history continues to exert a significant control on contemporary river form and process (Anderson & Jaeger, 2020; Collins & Montgomery, 2011; Scott & Collins, 2021). Understanding sediment delivery and storage in these valleys across a range of timescales will likely be important when assessing recent proglacial dynamics as a potential source of downstream river channel disturbance.

6 | CONCLUSION

We used a collection of high-resolution DEMs extending back to 1960 to assess geomorphic change in four proglacial watersheds on the flanks of Mount Rainier. We present three main conclusions.

First, recent deglaciation has triggered the evolution of disequilibrium valley floors towards more graded conditions. The cross-basin differences in initial valley floor gradients, and storage trends associated with any subsequent regrading, provide a primary explanation for the substantial cross-basin variations in erosion rates we observe.

Second, thresholds for motion are generally high, such that the timing and location of substantial erosion are dictated by extreme hydrological events and local confinement of flow. However, even major debris flow events may be modest in comparison to major rockfalls or lahars over long timescales.

Third, major sediment exporting events have generally created substantial deposits over the first several kilometers below the proglacial limits. These deposits have been remobilized relatively slowly.

Together, these results add to a body of work indicating that the short-term coarse sediment response to deglaciation is likely to be a function of the geometry of the exposed valley floor and fill, though likely modulated by the timing of stochastic extreme events. These findings generally underscore that, over periods of decades to centuries, relations between glacier retreat and sediment export are likely to be complex and may vary substantially across nominally similar watersheds in a given region. Factors controlling the storage or remobilization of deposits formed below the proglacial limits are likely to further modulate if, how, and when contemporary signals of proglacial sediment delivery are felt in downstream river systems.

ACKNOWLEDGMENTS

Any use of trade, firm, or product names is for descriptive purposes only and does not imply endorsement by the US Government.

DATA AVAILABILITY STATEMENT

The majority of the aerial imagery used in this study is openly available through the National Science Foundation's Arctic Data Center and at https://doi.org/10.18739/A2VH5CJ8K. Additional imagery was obtained from the US Geological Survey (USGS) Earth Explorer repository, at https://earthexplorer.usgs.gov/. Lidar data are openly available through the Washington Department of Natural Resource's lidar portal, available at https://lidarportal.dnr.wa.gov. Landsat metrics were derived from publicly available Landsat imagery courtesy of the USGS, and accessed through the Climate Earth Engine at https://climateengine.org. Climate data for the Paradise Ranger Station are openly available as part of the National Oceanic and Atmospheric Administration's Global Historic Climate Database, at https://www.ncdc.noaa.gov/cdo-web/datasets/GHCND/stations/GHCND:USC00456898/detail. Co-registered DEMs, shapefiles defining areas of analysis, and tabular summaries of topographic change, longitudinal profiles, and Landsat results are available in a USGS Data Release at https://doi.org/10.5066/P9056ZNG.

ORCID

Scott W. Anderson https://orcid.org/0000-0003-1678-5204
David Shean https://orcid.org/0000-0003-3840-3860

REFERENCES

Anderson, S.W. (2019). Uncertainty in quantitative analyses of topographic change: Error propagation and the role of thresholding. *Earth Surface Processes and Landforms*, 44(5), 1015–1033. https://doi.org/10.1002/esp.4551

Anderson, S.W. (2021). *Supporting datasets for proglacial topographic change analyses on mount rainier, 1960 to 2017*, Data Release. Reston, VA: US Geological Survey. https://doi.org/10.5066/P9056ZNG

Anderson, S.W., & Jaeger, K.L. (2020). Coarse sediment dynamics in a large glaciated river system: Holocene history and storage dynamics dictate contemporary climate sensitivity. *Geological Society of America Bulletin*, 133, 899–922. https://doi.org/10.1130/b35530.1

Anderson, S., & Pitlick, J. (2014). Using repeat lidar to estimate sediment transport in a steep stream. *Journal of Geophysical Research: Earth Surface*, 119(3), 621–643. https://doi.org/10.1002/2013JF002933

Antoniazza, G., & Lane, S.N. (2021). Sediment yield over glacial cycles: A conceptual model. *Progress in Physical Geography: Earth and Environment*, 0309133321997292. https://doi.org/10.1177/0309133321997292

Baewert, H., & Morche, D. (2014). Coarse sediment dynamics in a proglacial fluvial system (Fagge River, Tyrol). *Geomorphology*, 218, 88–97.

Ballantyne, C.K. (2002a). A general model of paraglacial landscape response. *The Holocene*, 12(3), 371–376. https://doi.org/10.1191/0959683602hl553fa

Ballantyne, C.K. (2002b). Paraglacial geomorphology. *Quaternary Science Reviews*, 21(18–19), 1935–2017. https://doi.org/10.1016/S0277-3791(02)00005-7

Beason, S.R. (2017). Change in glacial extent at Mount Rainier National Park from 1896 to 2015. Natural Resource Report NPS/MORA/NRR-2017/1472, National Park Service.

Betz, S., Croce, V., & Becht, M. (2019). Investigating morphodynamics on Little Ice Age lateral moraines in the Italian Alps using archival aerial photogrammetry and airborne lidar data. *Zeitschrift für Geomorphologie*, 62, 231–247.

Beyer, R.A., Alexandrov, O., & McMichael, S. (2018). The Ames stereo pipeline: Nasa's open source software for deriving and processing terrain data. *Earth and Space Science*, 5(9), 537–548. https://doi.org/10.1029/2018EA000409

Beylich, A.A., & Laute, K. (2015). Sediment sources, spatiotemporal variability and rates of fluvial bedload transport in glacier-connected steep mountain valleys in western Norway (Erdalen and Bødalen drainage basins). *Geomorphology*, 228, 552–567. https://doi.org/10.1016/j.geomorph.2014.10.018

Brardinoni, F., Picotti, V., Maraio, S., Bruno, P.P., Cucato, M., Morelli, C., & Mair, V. (2018). Postglacial evolution of a formerly glaciated valley: Reconstructing sediment supply, fan building, and confluence effects at the millennial time scale. *Geological Society of America Bulletin*, 130 (9–10), 1457–1473. https://doi.org/10.1130/B31924.1

Carrivick, J.L., & Rushmer, E.L. (2009). Inter-and intra-catchment variations in proglacial geomorphology: An example from Franz Josef Glacier and Fox Glacier, New Zealand. *Arctic, Antarctic, and Alpine Research*, 41(1), 18–36.

Carrivick, J.L., Geilhausen, M., Warburton, J., Dickson, N.E., Carver, S.J., Evans, A.J., & Brown, L.E. (2013). Contemporary geomorphological activity throughout the proglacial area of an alpine catchment. *Geomorphology*, 188, 83–95. https://doi.org/10.1016/j.geomorph.2012.03.029

Cavalli, M., Trevisani, S., Comiti, F., & Marchi, L. (2013). Geomorphometric assessment of spatial sediment connectivity in small alpine catchments. *Geomorphology*, 188, 31–41.

Cavalli, M., Heckmann, T., & Marchi, L. (2019). Sediment connectivity in proglacial areas. In Heckmann, T., & Morche, D. (Eds.), *Geomorphology of proglacial systems*. Berlin: Springer, pp. 271–287. https://doi.org/10.1007/978-3-319-94184-4_16

Church, M., & Ryder, J.M. (1972). Paraglacial sedimentation: A consideration of fluvial processes conditioned by glaciation. *Geological Society of America Bulletin*, 83(10), 3059–3072. https://doi.org/10.1130/0016-7606(1972)83[3059:PSACOF]2.0.CO;2

Church, M., & Slaymaker, O. (1989). Disequilibrium of Holocene sediment yield in glaciated British Columbia. *Nature*, 337(6206), 452–454. https://doi.org/10.1038/337452a0

Collins, B.D., & Montgomery, D.R. (2011). The legacy of Pleistocene glaciation and the organization of lowland alluvial process domains in the Puget Sound region. *Geomorphology*, 126(1–2), 174–185. https://doi.org/10.1016/j.geomorph.2010.11.002

Comiti, F., Mao, L., Penna, D., Dell'Agnese, A., Engel, M., Rathburn, S., & Cavalli, M. (2019). Glacier melt runoff controls bedload transport in alpine catchments. *Earth and Planetary Science Letters*, 520, 77–86. https://doi.org/10.1016/j.epsl.2019.05.031

Copeland, E.A. (2009). Recent periglacial debris flows from Mount Rainier, Washington. (Master's thesis).

Cossart, E. (2008). Landform connectivity and waves of negative feedbacks during the paraglacial period, a case study: The Tabuc subcatchment since the end of the Little Ice Age (Massif des Écrins, France). *Géomorphologie: Relief, Processus, Environnement*, 14(4), 249–260.

Cossart, E., & Fort, M. (2008). Sediment release and storage in early deglaciated areas: Towards an application of the exhaustion model from the case of Massif des Écrins (French Alps) since the Little Ice Age. *Norsk Geografisk Tidsskrift—Norwegian Journal of Geography*, 62(2), 115–131. https://doi.org/10.1080/00291950802095145

Cossart, E., Viel, V., Lissak, C., Reulier, R., Fressard, M., & Delahaye, D. (2018). How might sediment connectivity change in space and time? *Land Degradation and Development*, 29(8), 2595–2613.

Crandell, D.R. (1971). *Postglacial lahars from Mount Rainier volcano, Washington*, Professional Paper 677. Reston, MA: US Geological Survey. https://doi.org/10.3133/pp677

Crandell, D.R., & Fahnestock, R.K. (1965). *Rockfalls and avalanches from Little Tahoma peak on Mount Rainier, Washington*, Bulletin 1221-A. Reston, VA: US Geological Survey. https://doi.org/10.3133/b1221A

Curry, A.M., Cleasby, V., & Zukowskyj, P. (2006). Paraglacial response of steep, sediment-mantled slopes to post-"Little Ice Age" glacier recession in the central Swiss Alps. *Journal of Quaternary Science*, 21(3), 211–225. https://doi.org/10.1002/jqs.954

Czuba, J.A., Czuba, C.R., Magirl, C.S., & Voss, F.D. (2010). *Channel-conveyance capacity, channel change, and sediment transport in the lower Puyallup, White, and Carbon rivers, western Washington*, Scientific Investigations Report 2010-5240. Reston, VA: US Geological Survey. https://doi.org/10.3133/sir20105240

Czuba, J.A., Olsen, T.D., Czuba, C.R., Magirl, C.S., & Gish, C.C. (2012). *Changes in sediment volume in Alder Lake, Nisqually River basin, Washington, 1945–2011*, Open-File Report 2012-1068. Reston, VA: US Geological Survey. https://doi.org/10.3133/ofr20121068

Delaney, I., Bauder, A., Huss, M., & Weidmann, Y. (2018). Proglacial erosion rates and processes in a glacierized catchment in the Swiss Alps. *Earth Surface Processes and Landforms*, 43(4), 765–778. https://doi.org/10.1002/esp.4239

Dick, K.A. (2013). Glacier change in the North Cascades, Washington: 1900–2009. (Master's thesis).

Driedger, C.L., & Fountain, A.G. (1989). Glacier outburst floods at Mount Rainier, Washington State, USA. *Annals of Glaciology*, 13, 51–55. https://doi.org/10.3189/S0260305500007631

Driedger, C.L., & Kennard, P.M. (1986). *Ice volumes on cascade volcanoes: Mount Rainier, Mount Hood, Three Sisters, and Mount Shasta*, Professional Paper 1365. Reston, VA: US Geological Survey. https://doi.org/10.3133/pp1365

Esri (2020). ArcGIS pro (version 2.5).

Fahnestock, R.K. (1963). *Morphology and hydrology of a glacial stream: White River, Mount Rainier, Washington*, Professional Paper 422-A. Reston, VA: US Geological Survey.

Heckmann, T., & Vericat, D. (2018). Computing spatially distributed sediment delivery ratios: Inferring functional sediment connectivity from repeat high-resolution digital elevation models. *Earth Surface Processes and Landforms*, 43(7), 1547–1554. https://doi.org/10.1002/esp.4334

Heckmann, T., McColl, S., & Morche, D. (2016). Retreating ice: Research in pro-glacial areas matters. *Earth Surface Processes and Landforms*, 41(2), 271–276. https://doi.org/10.1002/esp.3858

Hock, R., Rasul, G., Adler, C., Cáceres, B., Gruber, S., Hirabayashi, Y., et al. (2019). High mountain areas. In Pörtner, H.-O., Roberts, D. C., Masson-Delmotte, V., et al. (Eds.), *IPCC special report on the ocean and cryosphere in a changing climate*.

Huntington, J., Hegewisch, K., Daudert, B., Morton, C., Abatzoglou, J., McEvoy, D., & Erickson, T. (2016). Climate engine: Cloud computing of climate and remote sensing data for enhanced natural resource monitoring and process understanding. *Bulletin of the American Meteorological Society*, 98, 2397–2409. https://doi.org/10.1175/BAMS-D-15-00324.1

James, M.R., & Robson, S. (2014). Mitigating systematic error in topographic models derived from UAV and ground-based image networks. *Earth Surface Processes and Landforms*, 39(10), 1413–1420. https://doi.org/10.1002/esp.3609

Knight, J., & Harrison, S. (2018). Transience in cascading paraglacial systems. *Land Degradation and Development*, 29(6), 1991–2001. https://doi.org/10.1002/ldr.2994

Konrad, C.P., & Dettinger, M.D. (2017). Flood runoff in relation to water vapor transport by atmospheric rivers over the western United States, 1949–2015. *Geophysical Research Letters*, 44(22), 11–456. https://doi.org/10.1002/2017GL075399

Lane, S.N., Bakker, M., Gabbud, C., Micheletti, N., & Saugy, J.-N. (2017). Sediment export, transient landscape response and catchment-scale connectivity following rapid climate warming and alpine glacier recession. *Geomorphology*, 277, 210–227. https://doi.org/10.1016/j.geomorph.2016.02.015

Leclercq, P.W., Oerlemans, J., Basagic, H.J., Bushueva, I., Cook, A.J., & Le Bris, R. (2014). A data set of worldwide glacier fluctuations. *The Cryosphere*, 8, 659–672. https://doi.org/10.5194/tc-8-659-2014

Legg, N.T., Meigs, A.J., Grant, G.E., & Kennard, P. (2014). Debris flow initiation in proglacial gullies on Mount Rainier, Washington. *Geomorphology*, 226, 249–260. https://doi.org/10.1016/j.geomorph.2014.08.003

Leonard, E.M. (1997). The relationship between glacial activity and sediment production: Evidence from a 4450-year varve record of neoglacial sedimentation in Hector Lake, Alberta, Canada. *Journal of Paleolimnology*, 17(3), 319–330. https://doi.org/10.1023/A:1007948327654

Lisle, T.E., & Church, M. (2002). Sediment transport–storage relations for degrading, gravel bed channels. *Water Resources Research*, 38(11), 1–1. https://doi.org/10.1029/2001WR001086

Mancini, D., & Lane, S.N. (2020). Changes in sediment connectivity following glacial debuttressing in an alpine valley system. *Geomorphology*, 352, 106987.

Meigs, A., Krugh, W.C., Davis, K., & Bank, G. (2006). Ultra-rapid landscape response and sediment yield following glacier retreat, Icy Bay, southern Alaska. *Geomorphology*, 78(3–4), 207–221. https://doi.org/10.1016/j.geomorph.2006.01.029

Menounos, B., & Clague, J.J. (2008). Reconstructing hydro-climatic events and glacier fluctuations over the past millennium from annually laminated sediments of Cheakamus Lake, southern coast mountains, British Columbia, Canada. *Quaternary Science Reviews*, 27(7–8), 701–713. https://doi.org/10.1016/j.quascirev.2008.01.007

Menounos, B., Hugonnet, R., Shean, D., Gardner, A., Howat, I., Berthier, E., et al. (2019). Heterogeneous changes in western North American glaciers linked to decadal variability in zonal wind strength. *Geophysical Research Letters*, 46(1), 200–209. https://doi.org/10.1029/2018GL080942

Micheletti, N., & Lane, S.N. (2016). Water yield and sediment export in small, partially glaciated alpine watersheds in a warming climate. *Water Resources Research*, 52(6), 4924–4943.

Micheletti, N., Lambiel, C., & Lane, S.N. (2015). Investigating decadal-scale geomorphic dynamics in an alpine mountain setting. *Journal of Geophysical Research: Earth Surface*, 120(10), 2155–2175. https://doi.org/10.1002/2015JF003656

Mills, H.H. (1978). Some characteristics of glacial sediments of Mount Rainier, Washington. *Journal of sedimentary research*, 48(4), 1345–1356. https://doi.org/10.1306/212F7685-2B24-11D7-8648000102C1865D

Nolan, M., Post, A.S., Hauer, W., Zink, A., & O'Neel, S. (2017). *Photogrammetric scans of aerial photographs of North American glaciers*. Santa Barbara, CA: Arctic Data Center. https://doi.org/10.18739/A2VH5CJ8K

Nuth, C., & Kääb, A. (2011). Co-registration and bias corrections of satellite elevation data sets for quantifying glacier thickness change. *The Cryosphere*, 5(1), 271–290.

Nylen, T.H. (2004). Spatial and temporal variations of glaciers (1913–1994) on Mt. Rainier and the relation with climate. (PhD thesis). https://doi.org/10.5194/tc-5-271-2011

O'Connor, J.E., & Costa, J.E. (1993). Geologic and hydrologic hazards in glacierized basins in North America resulting from 19th and 20th century global warming. *Natural Hazards*, 8(2), 121–140. https://doi.org/10.1007/BF00605437

Orwin, J.F., & Smart, C.C. (2004). The evidence for paraglacial sedimentation and its temporal scale in the deglacierizing basin of Small River Glacier, Canada. *Geomorphology*, 58(1–4), 175–202. https://doi.org/10.1016/j.geomorph.2003.07.005

Post, A. (1995). Annual aerial photography of glaciers in northwest North America: How it all began and its golden age. *Physical Geography*, 16(1), 15–26. https://doi.org/10.1080/02723646.1995.10642540

Reid, M.E., Sisson, T.W., & Brien, D. L. (2001). Volcano collapse promoted by hydrothermal alteration and edifice shape, Mount Rainier, Washington. *Geology*, 29(9), 779–782. https://doi.org/10.1130/0091-7613(2001)029<0779:VCPBHA>2.0.CO;2

Rolstad, C., Haug, T., & Denby, B. (2009). Spatially integrated geodetic glacier mass balance and its uncertainty based on geostatistical analysis: Application to the western Svartisen ice cap, Norway. *Journal of Glaciology*, 55(192), 666–680. https://doi.org/10.3189/002214309789470950

Roussel, E., Marren, P. M., Cossart, E., Toumazet, J.-P., Chenet, M., Grancher, D., & Jomelli, V. (2018). Incision and aggradation in proglacial rivers: Post-Little Ice Age long-profile adjustments of southern Iceland outwash plains. *Land Degradation and Development*, 29(10), 3753–3771.

Ryder, J.M. (1971). The stratigraphy and morphology of para-glacial alluvial fans in south-central British Columbia. *Canadian Journal of Earth Sciences*, 8(2), 279–298. https://doi.org/10.1139/e71-027

Schiefer, E., & Gilbert, R. (2007). Reconstructing morphometric change in a proglacial landscape using historical aerial photography and automated DEM generation. *Geomorphology*, 88(1–2), 167–178. https://doi.org/10.1016/j.geomorph.2006.11.003

Scott, D.N., & Collins, B.D. (2021). Frequent mass movements from glacial and lahar terraces, controlled by both hillslope characteristics and fluvial erosion, are an important sediment source to Puget Sound rivers. *Water Resources Research*, 57(4), e2020WR028389.

Scott, K.M., Vallance, J.W., & Pringle, P.T. (1995). *Sedimentology, behavior, and hazards of debris flows at Mount Rainier, Washington*, Professional Paper 1547. Reston, VA: US Geological Survey. https://doi.org/10.3133/pp1547

Shean, D.E., Alexandrov, O., Moratto, Z.M., Smith, B.E., Joughin, I.R., Porter, C., & Morin, P. (2016). An automated, open-source pipeline for mass production of digital elevation models (DEMs) from very-high-resolution commercial stereo satellite imagery. *ISPRS Journal of Photogrammetry and Remote Sensing*, 116, 101–117. https://doi.org/10.1016/j.isprsjprs.2016.03.012

Shugar, D.H., Clague, J.J., Best, J.L., Schoof, C., Willis, M.J., Copland, L., & Roe, G.H. (2017). River piracy and drainage basin reorganization led by climate-driven glacier retreat. *Nature Geoscience*, 10(5), 370–375. https://doi.org/10.1038/ngeo2932

Sigafoos, R.S., & Hendricks, E.L. (1972). *Recent activity of glaciers of Mount Rainier, Washington*, Professional Paper 387-B. Reston, VA: US Geological Survey. https://doi.org/10.3133/pp387B

Smith, L.C., Sheng, Y., Magilligan, F.J., Smith, N.D., Gomez, B., Mertes, L.A. K., et al. (2006). Geomorphic impact and rapid subsequent recovery from the 1996 Skeidarársandur Jökulhlaup, Iceland, measured with multi-year airborne lidar. *Geomorphology*, 75(1–2), 65–75. https://doi.org/10.1016/j.geomorph.2004.01.012

Turley, M. (2020). Exploring the importance of sediment disconnectivity and connectivity in glacierized catchments, Tahoma Creek, WA. (Master's thesis).

Walder, J.S., & Driedger, C.L. (1994). Rapid geomorphic change caused by glacial outburst floods and debris flows along Tahoma Creek, Mount Rainier, Washington, USA. *Arctic and Alpine Research*, 26(4), 319–327. https://doi.org/10.2307/1551792

Walder, J.S., & Driedger, C.L. (1995). Frequent outburst floods from South Tahoma Glacier, Mount Rainier, USA: Relation to debris flows, meteorological origin and implications for subglacial hydrology. *Journal of Glaciology*, 41(137), 1–10. https://doi.org/10.3189/S0022143000017718

Warburton, J. (1990). An alpine proglacial fluvial sediment budget. *Geografiska Annaler: Series A, Physical Geography*, 72(3–4), 261–272.

Xu, M., Bogen, J., Wang, Z., Bønsnes, T.E., & Gytri, S. (2015). Pro-glacial lake sedimentation from Jökulhlaups (Glof), Blåmannsisen, northern Norway. *Earth Surface Processes and Landforms*, 40(5), 654–665. https://doi.org/10.1002/esp.3664

Zemp, M., Hoelzle, M., & Haeberli, W. (2009). Six decades of glacier mass-balance observations: A review of the worldwide monitoring network. *Annals of Glaciology*, 50(50), 101–111. https://doi.org/10.3189/172756409787769591

SUPPORTING INFORMATION

Additional supporting information may be found in the online version of the article at the publisher's website.

How to cite this article: Anderson, S.W. & Shean, D. (2021) Spatial and temporal controls on proglacial erosion rates: A comparison of four basins on Mount Rainier, 1960 to 2017. *Earth Surface Processes and Landforms*, 1–22. Available from: https://doi.org/10.1002/esp.5274